Landslide monitoring using seismic ambient noise correlation: challenges and applications

Mathieu Le Breton, Noélie Bontemps, Antoine Guillemot, Laurent Baillet, Éric Larose

Landslide Monitoring Using Seismic Ambient Noise Correlation: Challenges and Applications

Mathieu Le Breton [a,b], Noélie Bontemps [a], Antoine Guillemot [a], Laurent Baillet [a], Éric Larose[a]
[a] Univ. Grenoble Alpes, CNRS, Univ. Savoie Mont-Blanc, IRD, IFSTTAR, ISTerre, 38000 Grenoble, France.
[b] Géolithe & Géolithe Innov, 38920 Crolles, France

This is the preprint accepted manuscript. The version published in Earth Science Reviews in May 2021 is acccessible at: https://doi.org/10.1016/j.earscirev.2021.103518

Abstract

Monitoring landslides is essential to understand their dynamics and to reduce the risk of human losses by raising warnings before a failure. A decade ago, a decrease of apparent seismic velocity was detected several days before the failure of a clayey landslide, that was monitored with the ambient noise correlation method. It revealed its potential to detect precursor signals before a landslide failure, which could improve early warning systems. To date, nine landslides have been monitored with this method, and its ability to reveal precursors before failure seems confirmed on clayey landslides. However three challenges remain for operational early-warning applications: to detect velocity changes both rapidly and with confidence, to account for seasonal and daily environmental influences, and to check for potential instabilities in measurements. The ability to detect a precursory velocity change requires to adapt the processing workflow to each landslide: the key factors are the filtering frequency, the correlation time window, and the choice of temporal resolution. Other optional processing steps are described, to better measure rapid velocity changes, improve signal-to-noise ratio, or estimate the measurement uncertainty. The velocity also fluctuates seasonally, by 1 to 6% on the reviewed landslide studies, due to environmental influences. This review reveals a linear trend between the amplitude of seasonal fluctuations and the filtering frequency over the 0.1–20 Hz range, encompassing both landslide and non-landslide studies. The environmental velocity fluctuations are caused mostly by groundwater levels and soil freezing/thawing, but could also be affected by snow height, air temperature and tide depending on the site. Daily fluctuations should also occur on landslides, and can be an issue when seeking to obtain a sub-daily resolution useful for early-warning systems. Finally, spurious fluctuations of apparent velocity—unrelated to the material dynamics—should be verified for. They can be caused by changes in noise sources (location or spectral content), in site response (change of scatterers, attenuation, or resonance frequency due to geometrical factors), or in inter-sensor distance. As a perspective, the observation of seismic velocity changes could contribute in as-

sessing a landslide stability across time, both during the different creeping stages occurring before a potential failure, and during its reconsolidation after a failure.

1 Introduction

Every year, slope destabilization events cause more than 4000 casualties and tens of billions of euros losses in material damage (Froude and Petley, 2018; Alimohammadlou et al., 2013). The risk can be reduced (Dai et al., 2002) by anticipating slope failures thanks to early-warning systems (Intrieri et al., 2012). These systems usually involve monitoring ground deformation, rainfall, or groundwater levels. Recently, geophysical methods have emerged as an alternative means to investigate the internal structure, hydrological and mechanical properties of landslides (Jongmans and Garambois, 2007), and to provide insights into their dynamics through monitoring (Fig. 1) (Whiteley et al., 2019). Electrical methods are mostly sensitive to the bulk material, pore-water salinity and water circulation, providing useful insights into the hydrological dynamics of the landslide. However, groundwater levels measured directly with piezometers cannot predict a rupture when used in isolation, therefore indirect estimations using geophysical methods are unlikely to provide better forecasts (Carrière et al., 2018a). Quadrature conductivity measurements on landslides (Flores Orozco et al., 2018; Gallistl et al., 2018) should provide complementary indicators on the characteristics of the solid matrix, such as the clay distribution and its permeability (Revil et al., 2020), but remain operationally difficult to permanently monitor with high accuracy. In contrast, passive seismic methods provide direct insights into the mechanical alterations of the subsurface that could lead to a failure. Passive seismic methods include site-specific spectral amplification, microseismic methods, and more recently ambient noise correlation. Analysis of long-term monitoring data using passive seismic methods has revealed clear precursory signals several hours or days before landslide failures (Larose et al., 2015).

The study of spectral amplification on a site consists in measuring and analyzing the horizontal-to-vertical ratio (H/V) of the seismic noise amplitude (Nakamura, 1989). Use of these techniques on landslides, especially for mapping, has been extensively reviewed (Del Gaudio et al., 2014; Kleinbrod et al., 2019). The method has been applied to rock columns (Lévy et al., 2010; Bottelin et al., 2013a), rock slopes (Burjánek et al., 2010, 2012; Kleinbrod et al., 2019), rock slides (Gaffet et al., 2010), and soft-material landslides (Amitrano et al., 2007; Méric et al., 2007; Danneels et al., 2008). It can be used for landslide zonation, either locally by mapping fractures and unstable areas (Burjánek et al., 2010; Häusler et al., 2019), or at a regional scale to assess the risk of earthquake-induced slope destabilization (Del Gaudio et al., 2014). The depth of a rock column fracture can be estimated by measuring the first resonance frequency together with the material's Young modulus (Valentin et al., 2017). The slid-

ing depth of a soft-material landslide that has a strong impedance contrast at its base can also be estimated from resonance frequencies combined with a rough shear-wave velocity profile (Imposa et al., 2017; Pazzi et al., 2017). In terms of precursory signals, the resonance frequency has been observed to decrease a few days before failure of a rock column (Lévy et al., 2010), or one hour before failure of a clay column (Fiolleau et al., 2020). However, this monitoring method appears adapted to sites with marked geometrical features, such as prone-to-failure columns, but is less adapted to monitor soft-soil landslides

Another family of methods, microseismic methods, has been used to monitor rockslides and softer material landslides, in order to detect events emerging from noise (Amitrano et al., 2007; Spillmann et al., 2007a), classify them (Walter and Joswig, 2008; Helmstetter and Garambois, 2010; Walter et al., 2011; Provost et al., 2017, 2018b; Vouillamoz et al., 2018), and locate them (Lacroix and Helmstetter, 2011; Provost et al., 2018a). For example, the method can be used to determine remotely the size, location, and timing of major failures and smaller afterslides (Schöpa et al., 2018). In terms of signals preceding a failure, the microseismic rate was found to correlate with the displacement rate of a rockslide (Spillmann et al., 2007b; Helmstetter and Garambois, 2010) or a soft-soil landslide (Amitrano et al., 2007; Walter et al., 2013; Tonnellier et al., 2013). This parameter may therefore serve as a proxy for displacement monitoring, making it possible to forecast the time-to-failure of a slope using common displacement-based methods (Intrieri et al., 2019). As for observed precursors, an increase in the microseismic rate was observed 2–15 hours before a cliff collapse or a rockfall (Amitrano et al., 2005; Senfaute et al., 2009), and a few hours or minutes before the failure of a suggested stick-slip landslide (Poli, 2017; Schöpa et al., 2018; Yamada et al., 2016). However, microseismic events (sometimes referred to as acoustic events when including high frequencies) are difficult to detect on soft-soil landslides, due to their low energy and strong attenuation, and in practice they cannot predict all failures.

Finally, the ambient noise correlation method —or passive seismic interferometry— (Sens-Schönfelder and Wegler, 2006; Sens-Schönfelder and Brenguier, 2019) has detected a drop in shear-wave velocity several days before the rupture of a clayey landslide (Mainsant et al., 2012b). Ambient noise correlation thus represents a potential new method that can detect precursors before a failure. It is promising because the drop in seismic velocity likely represents a decrease in rigidity (softening) in the underground layers, which is directly related to failure. Use of ambient noise correlation monitoring is increasing in landslide research: to date, nine landslides have been monitored (Renalier et al., 2010a; Mainsant et al., 2012b; Larose et al., 2015; Voisin et al., 2016; Bertello et al., 2018; Bièvre et al., 2018; Valentin, 2018; Colombero et al., 2018; Le Breton, 2019a; Guillemot et al., 2020; Bontemps et al., 2020; Fiolleau et al.,

2020) (Table 1). However, the method still encounters obstacles that appear to limit is applicability in early-warning systems. This review aims to identify the challenges, and their potential solutions, to integrating ambient noise correlation monitoring into an operational early-warning system.

The review starts by presenting the method and its applications on landslides, and by identifying its potential and limitations when included in a landslide early-warning system (part 2). The processing workflow and its key parameters are then presented (part 3). Fluctuations in the measurement may be caused by spatiotemporal variations of the noise field (part 4), or by environmental factors that appear crucial to understand (part 5). Finally, the influence of two major triggers—earthquakes and rainfall-induced fluidization—is presented, and their mechanisms discussed (part 6).

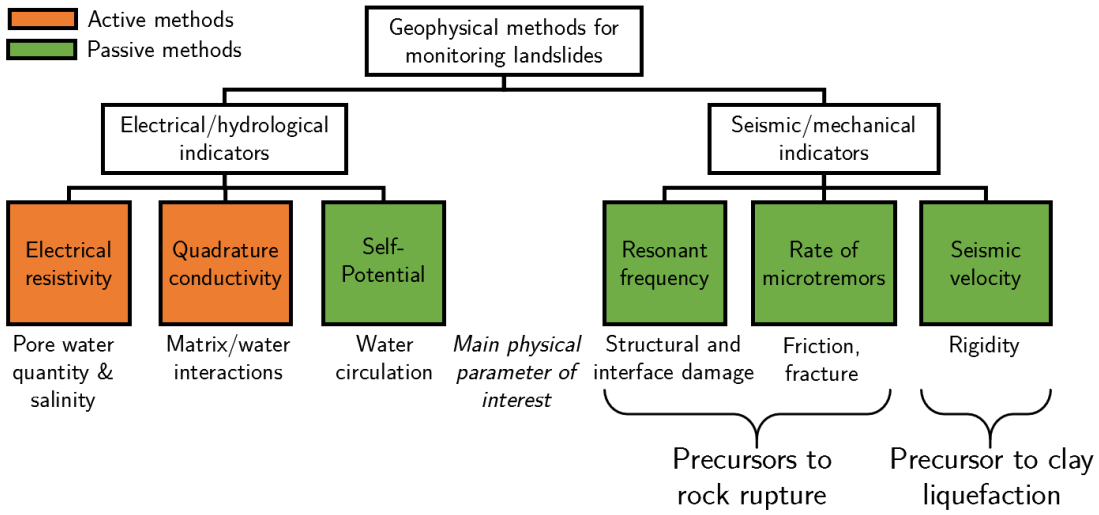

Fig. 1: Geophysical methods used to monitor landslides, adapted from Whiteley et al. (2019).

2 Ambient noise correlation for landslide monitoring

2.1 Ambient noise correlation

The basic premise of ambient noise correlation is to approximate the impulse response of medium to an excitation (or Green's function), by cross-correlating the seismic noise measured passively by two sensors. That results in a cross-correlation function (CCF) that is representative of the direct and diffused propagation within the medium. The method was first applied at a decimetric scale on a solid block using two ultrasonic receivers and a pulse generator (Lobkis and Weaver, 2001), then on at a crustal scale using the late seismic coda of an earthquake (Campillo and Paul, 2003). Exploiting the diffused ambient seismic noise from multiple sources then helped to reconstruct a more stable approximation of the Green's function (Shapiro and Campillo, 2004). The last two studies used reconstructions of the early-arrival direct surface waves (usually Rayleigh waves) to make the tomography of crustal ve-

locity. Subsequently, research teams suggested mixing the ambient noise correlation technique with coda wave interferometry, to detect small relative velocity changes in the coda. Thus, Sens-Schönfelder and Wegler (2006) proposed measuring relative variations in apparent velocity for crustal objects, such as a volcano, using the coda wave interferometry method. Over a year of monitoring, their data showed that an increase in groundwater levels reduced the apparent seismic velocity. Later, the apparent velocity was observed to decrease slightly before a volcanic eruption (Brenguier et al., 2011, 2008b, 2016; Obermann et al., 2013a; Nakata et al., 2016), or to decrease abruptly followed by a slow recovery after an earthquake (Wegler and Sens-Schönfelder, 2007; Brenguier et al., 2008a; Rivet et al., 2011; Hobiger et al., 2016). The apparent velocity was observed to decrease even more after an earthquake in a volcanic area (Brenguier et al., 2014; Taira and Brenguier, 2016). On smaller-scale objects, velocity decreases were observed when seepage occurred in dams or levees (Planès et al., 2016, 2017; Olivier et al., 2017) or during seasonal thawing of permafrost (James et al., 2017). In complement to apparent velocity, the indicator of CCFs decorrelation can detect structural changes of a material (e.g., Obermann et al., 2013; Walter et al., 2015; Preiswerk and Walter, 2018), which may also be used to monitor landslides (see 4.1).

2.2 Applications to landslide monitoring

On landslides, changes of apparent surface wave velocity can be monitored based on ambient noise correlation associated with coda wave interferometry. This technique attracted interest after detecting for the first time a clear velocity drop five days before the catastrophic acceleration of a shallow clayey landslide, at Pont-Bourquin (Mainsant et al., 2012b). This observation led to the development of a new technique to predict landslide failures. The drop in velocity, which reached 7% before the failure (Fig. 2), was attributed to a decrease in the rigidity of the soil during a partial fluidization at the base of the moving layer caused by an increase of water pore pressure. The variation of shear-wave velocity Vs depends on the densityρ and the rigidityμ, following the equation:

$$Vs = \sqrt{\frac{\mu}{\rho}} \tag{1}$$

This phenomenon was reproduced in laboratory experiments, where pore saturation was shown to decrease shear-wave velocity in the clay as the medium progressively fluidized (Mainsant et al., 2012a, 2015; Dong and Lu, 2016; Carrière et al., 2018a, 2018b) (see section 6.1).

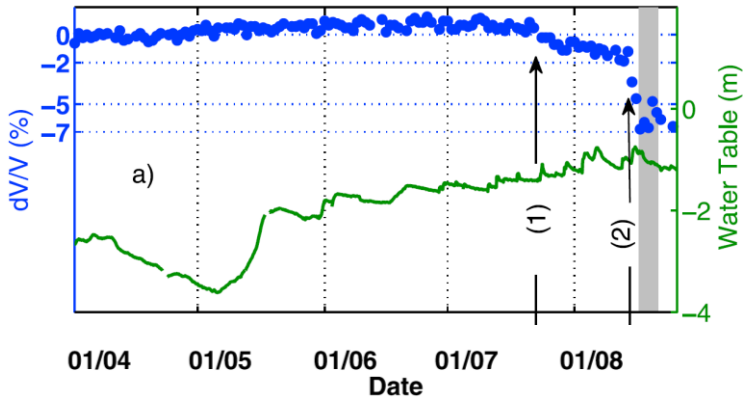

Fig. 2: On the Pont-Bourquin landslide, the apparent surface wave velocity (blue) was monitored before the major failure of 19 August 2010 (gray). Vertical line 1: the first velocity reduction starts after rainfall on 23 July and represents a 2% drop developing over 20 days. Vertical line 2: the major drop starts after rainfall on 14 August, with a total decrease of 7% over the 5 days preceding the landslide. The water table height (green) was not sufficient to predict a failure. From (Mainsant et al., 2012b).

Since then, several new landslides have been monitored with this technique (Table 1), including deep-seated landslides (Voisin et al., 2016; Bontemps et al., 2020), a rock glacier (Guillemot et al., 2020), and a rockfall/slide (Colombero et al., 2018). However, these landslides remained relatively stable over the course of their observation, and consequently no precursor signal was detected. A decrease in velocity related to a failure was observed on seven earthflows (Berti et al., 2019), but after the failure, since no data were recorded just before the failures. The potential of relative change in seismic velocity (called *dv/v*) to serve as a precursory signal was recently confirmed on Montevecchio earthflow (Bertello et al., 2018). In this latter study, the Rayleigh wave velocity decreased during the progressive acceleration of the landslide four days before its failure. In addition, on Harmalière rotational landslide, a progressive decrease in the CCF correlation coefficient (*CC*) was observed 20 days before the failure of an earth column (Fiolleau et al., 2020). In this study, one sensor was placed on the unstable column and the other was placed on stable ground. The decrease in *CC* was probably due to the progressive opening of the rear fracture.

Table 1: Landslide monitoring based on ambient noise correlation. Landslide monitoring studies of short duration or low time resolution were not included (Chtouki et al., 2017; Harba and Pilecki, 2017; Hussain et al., 2019)

Landslide	Technique (a)	Precursor	Seasonal variation	Duration (yr.)	Sliding depth (m)	Slide class (Hungr, 2014)	References
Avignonet, France	dv/v	na	±0.5%	2.5	10–16 and 42–47	Clay/silt compound slide	(Renalier et al., 2010a)
Pont-Bourquin, Switzerland	dv/v	2–7% in 5 d, at 10–12 Hz	±2%	6	10	Clay planar slide-earthflow	(Mainsant et al., 2012b; Larose et al., 2015; Bièvre et al., 2018; Le Breton, 2019a)
Utiku New Zealand	dv/v	na	±2%	1.1	300 (Massey et al., 2013)	Planar rock-slide/earthflow	(Voisin et al., 2016)
Madonna del Sasso, Italy	dv/v H/V	na	±10% 2.7-3.3 Hz	2.3	15	Rock fall-slide	(Colombero et al., 2018)
Harmalière, France	CC H/H	0.8–0 in 20 d 9–6 Hz in 8 h	na na	0.3	3	Earth rotational slide	(Fiolleau et al., 2020)

Gugla, Switzerland	dv/v CC	na na	±1.5% 1-0.5	3	2–15	Rock slope deformation/creeping	(Guillemot et al., 2020)
Maca, Peru	dv/v	Na	±1%	3	50	Clay/silt compound slide	(Bontemps et al., 2020)
Montevecchio, Italy	Time lapse dv/v	After event: 30% at 11 Hz	na	1.3	unknown	Earthflow	(Bertello et al., 2018)
Char d'Osset, France	dv/v	Na	±2.5%	2	≈15	Debris flow	(Valentin, 2018, chap. 7)

2.3 Challenges for early-warning system applications

(a) dv/v: relative temporal velocity variations based on the coda of the Green's function; CC: Correlation Coefficient of the Green's function. H/V and H/H use ambient noise to monitor the horizontal resonance frequency, normalized relative to the vertical or horizontal component from another sensor.

Landslide early-warning systems (Intrieri et al., 2012) could take advantage of ambient noise correlation monitoring. Firstly, the method measures the loss of rigidity that causes the failure directly in the material's bulk, at depth. It is therefore complementary to the indicators of surface displacement or rainfall infiltration that are commonly monitored. Secondly, ambient noise correlation provides continuous and robust monitoring even under rain, snow, vegetation, or without a line of sight between sensors. Thirdly, sensor can be installed either on the stable or unstable part of the slope, at the surface, or partially buried, and do not require drilling unlike underground piezometers or inclinometers.

Nevertheless, an early-warning system must predict a failure before it occurs, which adds several challenges compared to the existing applications in the literature. Firstly, all failures should be detected, with a low rate of false alerts. So far, failures were reported on three landslides monitored with an ambient noise correlation method, and all showed a precursory signal (Mainsant et al., 2012b; Bertello et al., 2018; Fiolleau et al., 2020). In particular, the Pont-

Bourquin landslide showed no false alert during 5 years without failure (Bièvre et al., 2018), using a ±2.5 % threshold value. The threshold must be carefully adapted to each landslide, to remain higher to the seasonal fluctuations of *dv/v* (to avoid false alerts) and lower than the precursory signal. A preliminary monitoring period is therefore required before setting a threshold.

Secondly, the detection system should work without fine-tuning the processing parameters based on the data obtained after the failure. Therefore, prior knowledge of the landslide's behavior is important to set appropriate parameters in the processing workflow. A depth-sensitivity analysis constrains processing parameters such as the frequency range of the seismic signal and time window for the coda (detailed in section 3). This requires a first investigation to estimate the active layer's depth —subject to rigidity reduction— and its seismic velocities.

Finally, an alarm should be raised early enough (=long lead time) before a potential landslide failure, to give time for mitigation measures (Intrieri et al., 2012). Today, the state-of-the-art time resolution for landslide monitoring is 1 day (Mainsant et al., 2012b), which corresponds to a delay of 2+ days before detection in order to confirm the measurement in case of an outlier. The delay can be reduced by using a fully automated processing (e.g., Duputel et al., 2009, on a volcano), by reducing the time resolution to less than one day (even though we must then contend with daily cyclic variations and a lower signal-to-noise ratio), and by rectifying reversible environmental influences to allow for a more sensitive threshold. Today, the delay of the method restricts its usage in early warning systems to slopes evolving over long time scales—several days or weeks.

3 Processing for early-warning systems

3.1 Processing workflow

A general processing workflow is presented in Fig. 3, based on those proposed by Bensen et al. (2007), Larose et al. (2015), Sens-Schönfelder and Brenguier (2019), and Ritzwoller and Feng (2019).

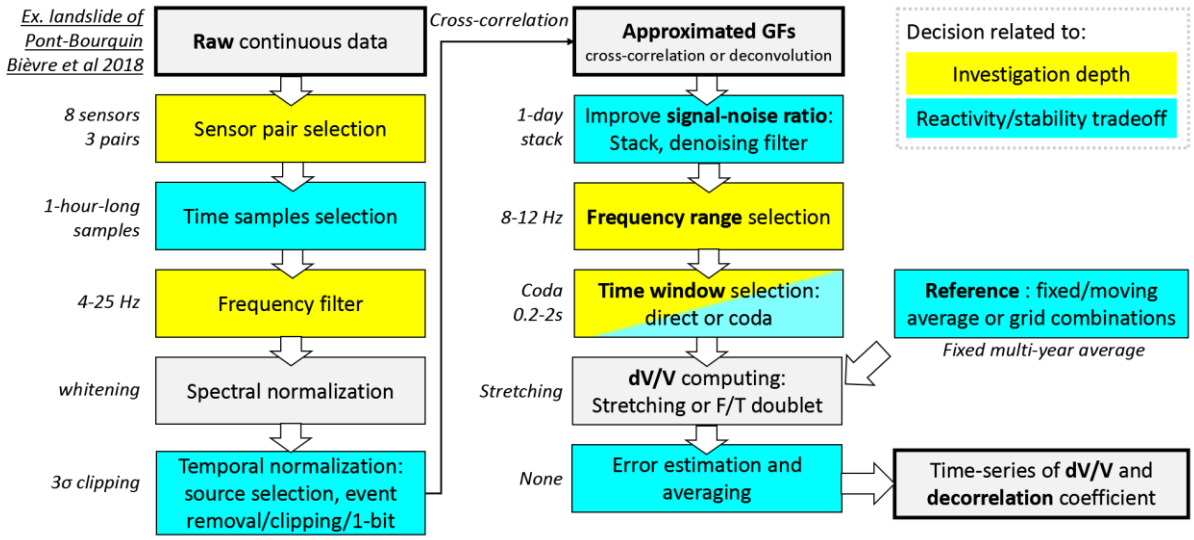

Fig. 3: General workflow to process ambient seismic noise correlation and extract daily relative velocity changes *dv/v* and correlation coefficients *CC*. Adapted from Larose et al. (2015).

The workflow starts with preparation of the continuous raw data (or "traces") recorded by the seismometers. Traces consist of velocity or acceleration records usually in the vertical or in the three directions. Data is typically sampled every 1–10 milliseconds and accurately timed by a GPS-synchronized clock to avoid a time drift (Sens-Schönfelder, 2008; Stehly et al., 2007). Sensors are selected in pairs within the area investigated. Their traces are split in time into subrecords of equal duration. The duration chosen for these segments, typically one hour, determines the shortest possible resolution of the *dv/v*. Each *i* trace segment is then filtered within a broad frequency band, and the contribution from each frequency can be equalized with a whitening operation (Bensen et al., 2007; Fichtner et al., 2017). The traces spectrum can be normalized in the frequency domain, and filtered using an apodization window shaping a smooth transition from 0 —outside the bandwidth— to 1 —within the bandwidth:

$$S_i^{\text{filtered}}(\omega) = \frac{S_i^{\text{raw}}(\omega)}{\left|S_i^{\text{raw}}(\omega)\right|} A^{f_{\min}, f_{\max}}(\omega) \tag{2}$$

The next step consists in removing strong events, such as earthquakes, that emerge from the noise. Stronger events can be attenuated in the time domain by applying a moving-average weighted normalization (Bensen et al., 2007), or by clipping the signal once or iteratively (Machacca-Puma et al., 2019a) above a maximum threshold value. The threshold can be a percentile of the amplitude or be based on the sign of the signal measured (one bit) (Larose, 2004). All these methods increase the contribution of scattered waves (very stable) and continuous weak sources (often stable) compared to strong transient events, and thus provide more stable CCFs.

The CCFs are then computed by cross-correlating the traces from d sensors. Cross-correlating two traces and provides an approximation (rigorously speaking, the time derivative) of the Green's function between the two sensors that recorded them:

$$h_{AB}(\tau) \approx CCF_{AB}(\tau) = \int a(t)b(t+\tau)dt \quad (3)$$

Alternatively, the Green's function can be estimated by applying deconvolution instead of cross-correlation (Mehta et al., 2007; Snieder and Safak, 2006; Joubert et al., 2018). This has provided a more stable estimation of the Green's function when using borehole sensors or unstable sources (Nakata and Snieder, 2012).

CCFs can then be normalized by the energy of their traces before stacking, generally over one or several days. CCFs are then filtered within the frequency range investigated, within often a more narrow band than the initial broad-band filtering. Each CCF is then compared to a reference CCF (e.g., the average CCF over the whole monitoring period, see 3.3.4). The *dv/v* between these two CCFs is computed within a given time window, using either the stretching or the doublet method. The doublet method (Ratdomopurbo and Poupinet, 1995; Brenguier et al., 2008b) consists in measuring the time shift between two similar signals over a narrow moving window—in time or frequency domain—and extracting the slope (Fig. 4.a). In contrast, the stretching method (Sens-Schönfelder and Wegler, 2006) consists in simulating an artificial seismic velocity change by stretching the wavelet through the factor and applying the transformation. The CCFs are stretched for several possible values of (Fig. 4.b). The optimum velocity change *dv/v* at a given date maximizes the *CC* computed between the stretched and reference CCF values.

$$CC(\varepsilon) = \frac{\int h\left((1-\varepsilon)\times t\right) h_{ref}(t)dt}{\sqrt{\int h\left((1-\varepsilon)\times t\right)^2 dt \int h(t)^2 dt}} \quad (4)$$

The two methods were compared by Hadziioannou et al. (2009). The comparison revealed the doublet method to be better for eliminating localized decorrelation of the waveforms, identifying nonlinear velocity variations across time windows, and providing the same contribution from every part of the CCF whatever its amplitude. In contrast, the stretching method works with a lower signal-to-noise ratio and requires less parametrization, which seems better adapted for use in an automatic early-warning system.

This processing can be applied to multiple pairs of sensors, providing multiple *dv/v* time series measured between each pair. These spatialized measurements can be used to locate the velocity change (Brenguier et al., 2008b), or to compute the mean and standard deviation of the *dv/v* over the whole area covered by the sensors.

The main settings of the processing workflow are the stacking time, frequency range, reference selection, and time window. Choosing the adequate settings depend on the investigated site and on the need to measure either a stable or rapidly moving *dv/v*, which is discussed in the following sections..

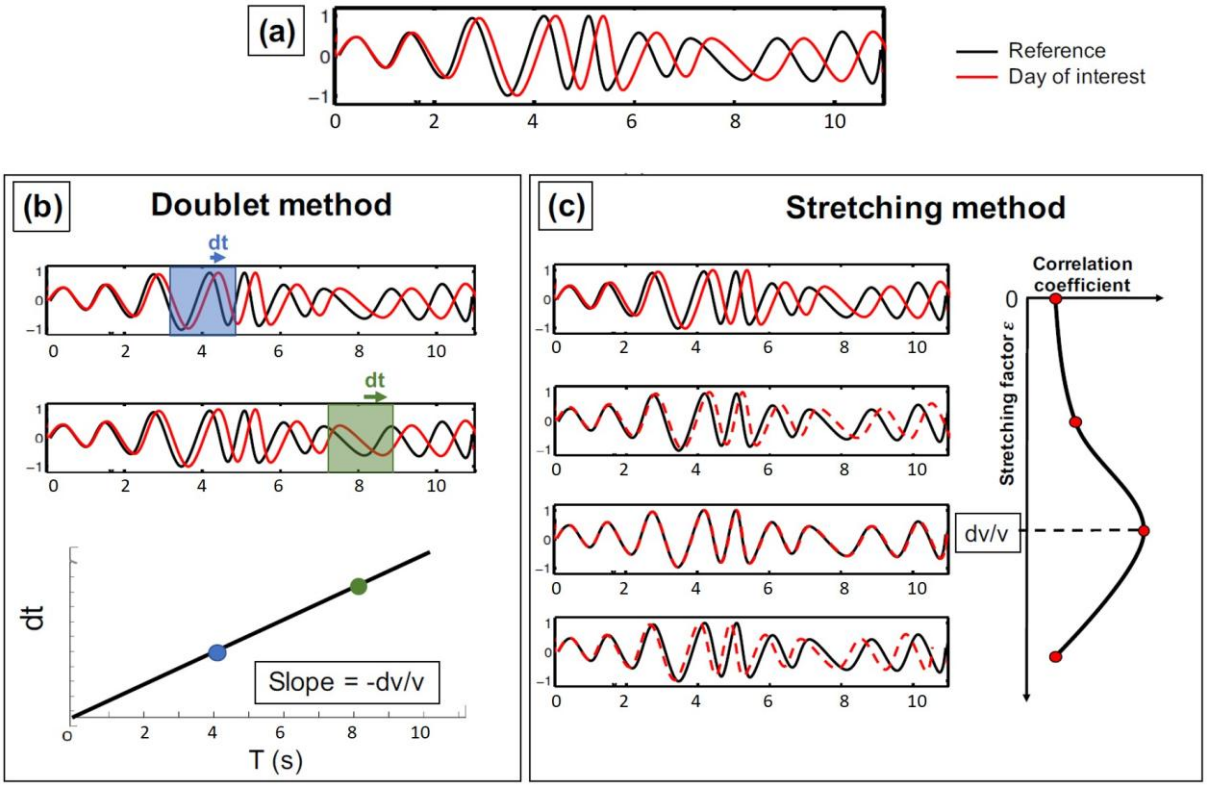

Fig. 4: Illustration of (b) doublet and (c) stretching methods, used to estimate a *dv/v* value from a sample signal (a), modified from (Hadziioannou, 2011; Hadziioannou et al., 2009)

3.2 Investigation depth

The diffuse propagation between two sensors, represented by the CCF, involves body and surface waves. These waves, that mutually convert due to heterogeneities beneath the free surface (Shapiro et al., 2000; Larose et al., 2005; Margerin et al., 2009), exhibit very different sensitivity depths (Obermann et al., 2013b). This section investigates the contributions of body and surface waves to the apparent *dv/v*, depending on the depth and properties of the medium.

The surface waves considered in the literature and in this review are mostly Rayleigh waves, because vertical sensors are generally used. In a multilayer terrain, the phase velocity of these waves depends on their frequency—they are dispersive. The investigation depth z_{max} of Rayleigh waves—which is generally shallower than body waves—is approximately one third of the maximum wavelength (e.g., Park et al., 1999). The maximum wavelength depends on the phase velocity at the lowest signal frequency. The phase velocity, in turn, depends on the vertical profile of body wave velocities and on the density of the medium. Therefore, an accurate computation of the depth sensitivity as a function of frequency (e.g., Fig. 5) requires all three parameters (V_S, V_P, and density) to be modeled at depth. On landslides, the frequency filtering of the CCFs must therefore be defined as a function of the depth and the nature of the whole unstable layer. The sensitivity depth of a velocity change can be estimated from the dispersion of direct surface wave velocities, i.e., surface wave phase velocity versus frequency. The curve is then inverted to estimate the shear-wave velocity profile at depth (Wathelet et al., 2008), using for example the active MASW or passive ReMI method (Park et al., 1999; Louie, 2001). Shear-wave velocity tomography based on CCFs has been reported for a few landslides (Renalier et al., 2010b; Pilz et al., 2014; Harba and Pilecki, 2017; Harba et al., 2019), and results are similar or complementary to active methods.

As an example of depth sensitivity, the frequency dependence of *dv/v* was used to estimate the depth of the liquefied medium during the Pont-Bourquin failure (Mainsant et al., 2012b), and to estimate fluctuations in groundwater levels on the Utiku landslide (Voisin et al., 2016). Information on the landslide's sliding depth and the seismic velocity of its layers will help to select in advance the frequency to be monitored in the cross-correlations.

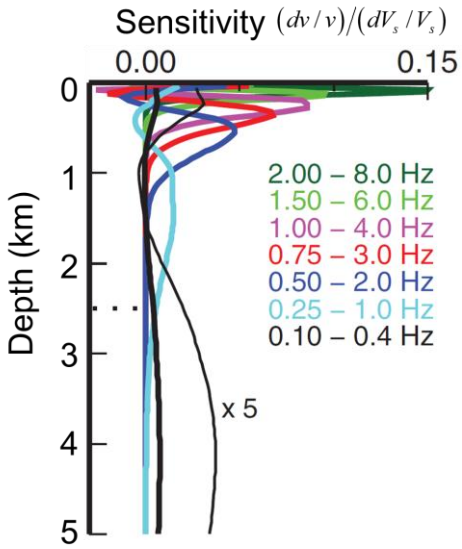

Fig. 5: Example showing the sensitivity of the Rayleigh phase velocity to shear velocity perturbation dV_s over a thin layer, for various frequency ranges, computed for the Deep Heat Mining Project in Basel, Switzerland. The 0.1 − 0.4 Hz curves, in black, are magnified x5. Adapted from (Hillers et al., 2015).

Scattered waves are composed of both P and S body waves (Hennino et al., 2001). They are sensitive at deeper levels than surface waves. Their sensitivity depth can be estimated using the diffusion approximation (e.g., Wegler and Lühr, 2001). Alternatively, the radiative transfer approximation can be used (Paasschens, 1997) and appears more accurate at shallow depths (Obermann et al., 2013b). The depth sensitivity defined by radiative transfer depends on the energy velocity, on the distance between the source and receiver, and on the scattering mean free path. The scattering mean free path—the average wave distance between two scattering events—is controlled by the medium's degree of heterogeneity. The time window observed for the CCF also plays a key role, as body waves dominate at later times (say, about six mean free times, representing the propagation over six mean free paths). Therefore, the sensitivity depth of body waves depends on the medium's heterogeneity, on the inter-sensor distance and on the processing parameters (time window). In practice, attenuation by the medium also plays a role, as does the frequency which influences both the attenuation and the degree of heterogeneity: lower frequencies will be less sensitive to small heterogeneities, but also less attenuated. In short, investigations at shallow depths (i.e., of landslides) based on body waves would require a highly heterogeneous medium, a late time window, and a high frequency. The hypothesis that body waves dominate the *dv/v* results has not been tested in landslide studies, but these waves might still contribute in part to the *dv/v*.

The relative contributions of body and surface waves were simulated in 2D and 3D by Obermann et al. (2013, 2016, 2019). Fig. 6 shows the contribution of surface waves (in red) and body waves (in blue) to the apparent velocity change dv/v_{app} in response to a bulk velocity

change dv/v_{bulk} within a layer located at a variable depth, in an ideal lossless medium. This model indicates that surface waves are sensitive down to about half a wavelength, and that scattered body waves are sensitive at much greater depths. However, the distribution between body and surface waves' sensitivity depends not only on the depth of the velocity change, but also on the time window selected and on the mean free path. Surface waves dominate early coda (early scattered waves), whereas bulk-diffused waves dominate later coda. We suspect that this bulk diffusion regime (P/S) occurs when absorption is weak compared to scattering. However, in metric and hectometric landslides, seismic waves generally have a relatively high frequency and the shallow material is highly absorbing. Consequently, very late coda are barely visible and the bulk diffusion regime is relatively rarely implicated in field experiments. In contrast, in very large landslides or rock slopes (> kilometric scales), this regime might play a role. Furthermore, controlling the contribution and sensitivity depth of bulk-diffused waves will require estimation of the transport mean free path of the material, which is rarely measured. In practice, the time window is set between the end of the high-amplitude direct surface waves, up to 5–10 periods of the selected frequency or the limit before the CCF becomes too noisy. In summary, the role of surface waves is sufficient to monitor landslides based on coda wave interferometry, but the effect of body waves should be kept in mind when studying very large landslides.

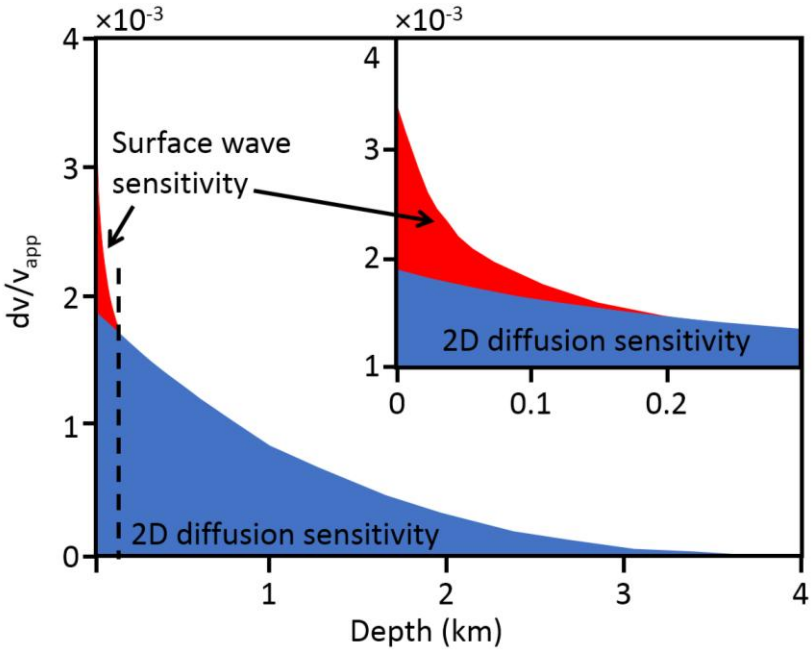

Fig. 6: Simulation of the apparent velocity variations caused by a 20% increase in bulk velocity in a 200-m thick layer at depth, depending on the depth of the layer (S-wave velocity of the ground = 3750 m/s, frequency range of the ambient noise =16 − 24 Hz, stretching time window = 2.8 − 4.4 s). Surface waves appear sensitive to changes near the surface (in red, up to approximately half the wavelength) whereas diffused waves (in blue) are sensitive to much deeper changes (in blue). Redrawn from (Obermann et al., 2013b).

3.3 Stability, responsiveness, and signal-noise ratio

Today, CCFs on landslides are averaged over 24 h or more. This period can be too long for landslide early-warning systems that often require decisions to be made just a few hours or days before a potential failure. The ability to monitor rapid *dv/v* variations, with subdaily time resolution, is required to observe landslide processes (e.g., water infiltration). However, decreasing the time resolution often degrades the signal's stability or its signal-to noise ratio due to the limited signal stacking. A tradeoff is thus required between signal stability and the time resolution. This tradeoff implies several decisions: using small or large number of noise sources, ballistic or scattered waves, short or long stacking periods, and multiple or unique reference(s). All these options are detailed in the following subsections.

3.3.1 Localized or diffuse sources

Seismic signals used for ambient noise correlation may originate from strong transient events, repeating localized sources, or weak distributed sources. Reconstructing a Green's function requires sources that perfectly surround the pair of sensors, a homogeneous spatial distribution of sources around the sensors, or a highly scattering medium (scatterers act as secondary sources). Green's function reconstruction was first tested using the coda (=late arrival) from regional earthquakes, occurring at multiple locations (Campillo and Paul, 2003). One drawback of this method is the limited number of sources and the limited available coda (limited scattering versus attenuation effects). Without scattering, reconstruction of the direct waves requires the seismic sources to be aligned with the two sensors to achieve correlation (Snieder and Larose, 2013). In practice, these very restrictive conditions are rarely met, but a stable CCF is sufficient to monitor relative velocity changes (Hadziioannou et al., 2009), which simply requires stable sources from one stacking period (generally 24 h) to the next. This latter condition is met in most field applications, making it possible to retrieve *dv/v* (but not the full Green's function, strictly speaking).

Near-surface applications can also exploit smaller repeating sources that are stable in space and frequency, such as cars passing on a road (Planès et al., 2017). The sources must be first selected and identified—and their spatial and spectral stability verified—either by their time-domain signature, frequency-domain signature, or spatial/azimuthal signature (Preiswerk and Walter, 2018). If the sources identified move slightly in space or frequency, a small phase shift will be visible in the correlograms resulting in false *dv/v*. The verifications required are

complicated for continuous monitoring, as they require human validation, and should be avoided as much as possible within an early-warning system, but in some industrialized areas there is no other option.

The contribution of continuous and weak noise can be greatly increased by removing strong sources. In such case, the ambient noise may come either from continuous weak sources (e.g., wind, rivers, trees) or from secondary sources due to waves being scattered multiple times before arriving on the sensor. Scattered sources will ensure a better spatial distribution of the pseudo-sources (scatterers should surround the sensors) as well as better stability: underground scatterers out of the landslide rarely move, and act like stable secondary sources, thus contribute to stability. Potential moving scatterers inside the landslide contribute to decorrelation (thus instability of the reconstructed GF, see 4.1) but this population is in limited (and minor) number. In practice, scattered waves are continuous in time but have a low amplitude, and they may be eclipsed by strong events. The contribution of stronger events to the CCF can also be removed by clipping (see section 3.1). The influence of source instability over time, and how to reduce it, is discussed in section 4.1.

3.3.2 Scattered or ballistic waves

Ballistic waves (early arrivals in the correlograms) have a stronger signal than scattered waves (coda of the correlograms) but are more strongly affected by minor changes to the source direction or by small alterations occurring at the ground surface between the two sensors. The emergence of scattered waves in the correlations improves stability but requires a better signal-to-noise ratio and a longer observation time than when reconstructing ballistic waves. It is not always straightforward to discriminate between ballistic and scattered waves. Direct and scattered waves can be distinguished after the slower arrival time, plus an additional time corresponding to the time duration for the source ($1/\Delta f$, where Δf is the frequency bandwidth). Furthermore, it is easier to measure velocity variations using long coda from scattered waves (more than 10 periods of the filtered frequency) rather than short early arrivals. Exploiting multiple periods provides a more accurate estimation of waveform time shifts, and using broad time delays t allows more accurate computation of dv/v (particularly for landslide applications where short inter-sensor distances cause ballistic waves to arrive at times close to zero). Scattered waves are used more frequently, but ballistic waves can also be exploited (e.g., Voisin et al., 2016). Computing the dv/v on the full cross-correlations, including very early CCF times, would include both contributions, but the higher amplitude of the ballistic wave may dominate when using the stretching method. Alternatively, the doublet method does not suffer from the domination of large-amplitude early arrivals because it uses

constant weighting throughout the moving window. The technique used to compute *dv/v* must be carefully selected depending on what type of waves are to be used.

3.3.3 Stacking and denoising

Reducing the time resolution below 24 h reduces the signal-to-noise ratio of the CCFs (Hadziioannou et al., 2011) and can introduce rapid sub-daily *dv/v* fluctuations of potentially a few % (see 5.2, Fig. 14 and Table 3). These fluctuations are not easy to handle in terms of processing, and might combine true velocity variations with spurious variations due to anthropogenic noise fluctuations (see 3.3.1). The time resolution could be improved in spite of daily fluctuations by stacking the hourly cross-correlations over a 1-day moving average window, but this cannot truly be considered to be a sub-daily resolution due to its low-pass filtering effect. This approach was used for example to automatically monitor a volcano, with a 10-days moving average window (Duputel et al., 2009). Alternatively, a reference CCF could be computed separately for each period of the day (e.g., each hour) and compared with each CCF for the same period (variant of Richter et al., 2014). The stacking period that provides a high enough signal-to-noise ratio can be estimated using a convergence analysis (e.g., Joubert et al., 2018). Additionally, the signal-to-noise ratio can be increased using an SVD-Wiener filter to remove noise that is not coherent between neighboring CCFs (Moreau et al., 2017). Finally, fluctuations could be reduced by subtracting a model predicting their occurrence from the *dv/v* curve, based on meteorological data or by filtering out long period variations (e.g., Gassenmeier et al., 2016; Bottelin et al., 2017)

3.3.4 Reference CCFs

Selecting the reference CCF affects the ability to measure rapid or strong variations. Most studies compare each CCF to a single reference CCF, obtained by stacking all the CCFs over the whole period investigated, or over a selected stable period. Stacking has the advantage of increasing the signal-to-noise ratio, and using a single reference has the advantage of ensuring consistency between all the *dv/v* computed. However, CCFs may evolve over time, due to changes in the sources or in the structure of the material observed. Consequently, stacking CCFs that are not consistent over time may induce bias within the averaged CCF, and could decrease the accuracy of the *dv/v* computation.

Computing a reference in two iterative steps increases the *dv/v* accuracy when the velocity varies considerably (Richter et al., 2014). First, an intermediate *dv/v* is first computed using a standard reference. This *dv/v* value is used to normalize the velocity of each CCF and increase mutual coherence. A second reference, more coherent, is obtained by stacking the corrected CCFs, and used to compute the final *dv/v*. This method is used for example to tackle cycle-skipping problems (Richter et al., 2014). Cycle-skipping is a common drawback of *dv/v* com-

puting methods: it may create large instantaneous *dv/v* jumps or miss resolving a rapid variation in *dv/v* (e.g., the gray rectangle in Fig. 8). The phenomenon may occur both with the stretching method, due to picking the wrong maximum for the *CC*, and with the doublet method, due to incorrect phase unwrapping. This problem is more common with rapid *dv/v* variations, when the signal-to-noise ratio for cross-correlations is low, when testing for a large range of velocity variations during stretching, or when using small time windows, late time windows, and high frequency ranges.

Sometimes, changes in the structure of the medium (including scatterer positions) alter the waveforms so much that they are too dissimilar to be accurately compared. Computing a moving-window reference, over only several days to months period before the day of interest, can minimize this unwanted effect. On permafrost for example, thawing strongly alters the correlation over time. In that case, computing the reference over a moving window (3 to 10 days' long) allows rapid velocity variations to be resolved (James et al., 2017). However, such method can introduce a long-term *dv/v* drift (due to the accumulation of small errors) that requires an additional correction. The method may also result in a lower signal-to-noise ratio caused by the shorter stacking period of the reference.

$\left[\frac{\delta v}{v}(t_i)\right]_{i,j} = \left[\frac{\delta v}{v}\right]_j - \left[\frac{\delta v}{v}\right]_i$

i, *j* the final method consists in computing the *dv/v* between every possible pair of dates , resulting in a 2-D grid of velocity variations . The optimal 1-D *dv/v* time series of is then inverted to fit the grid (Brenguier et al., 2014; Machacca-Puma et al., 2019b) (see Fig. 7). This technique could handle a reduction in the correlation coefficient between CCFs over time by giving a higher weight is given to mutually coherent CCFs (potentially close in time). It also accounts for CCF pairs that are distant in time to avoid a drift. This may result in the best responsiveness/stability tradeoff, but at the cost of greater computational complexity.

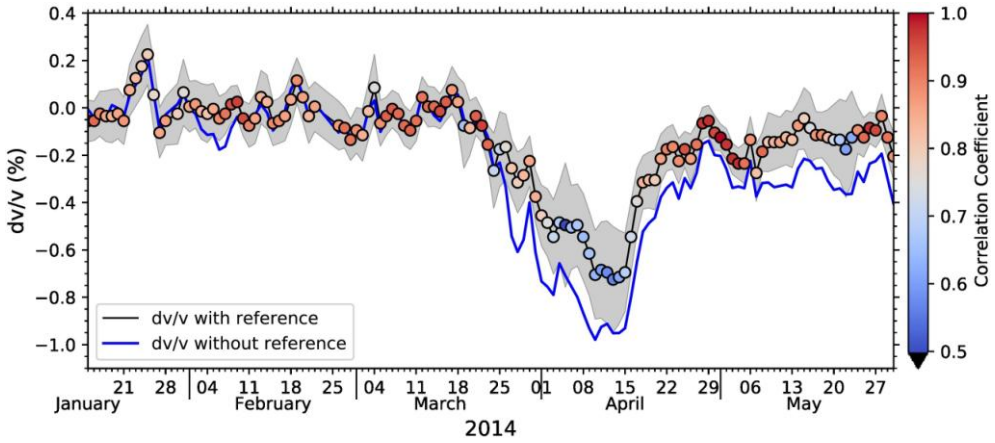

Fig. 7: Comparison of an inverted *dv/v* time series to the standard stretching method, and to the full *CC* matrix, from (Machacca-Puma et al., 2019b)

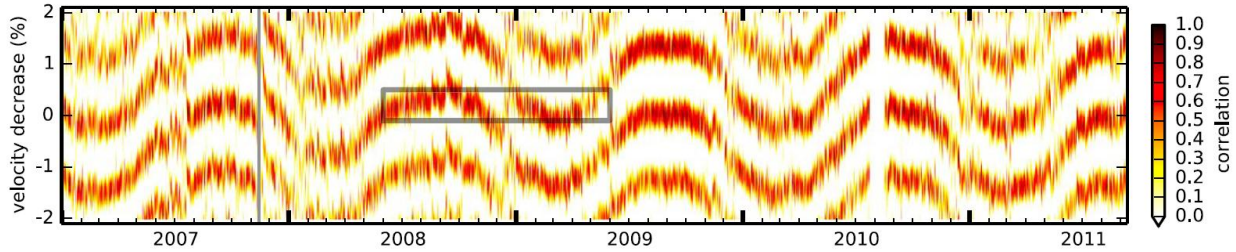

Fig. 8: Correlation coefficient between the CCFs, when testing for velocity variations during stretching. The *dv/v* is at the maximum correlation coefficient. The image emphasizes potential aliasing problems after a sudden *dv/v* change, highlighted by the vertical gray line (earthquake) and the gray box. Rapid velocity changes may be better resolved using an iterative reference (Richter et al., 2014).

3.4 Assessing uncertainty

A reliable warning system using *dv/v* observations requires to estimate their uncertainty, in order to avoid false warnings due to artifacts or low-quality data. To ensure the stability of the cross-correlations over time, its *CC* can be computed relative to the reference, or even between each pair of sensors (Lesage et al., 2014). CCFs with a low correlation coefficient (typically < 0.6) may be omitted from the *dv/v* computation to avoid computing erroneous velocity variations. Another indicator of quality is the spatial homogeneity and stability of the sources, which can be estimated from the consistency between the positive and negative sides of the cross-correlations (e.g., Brenguier *et al.* 2008a), or between different station pairs with distinct azimuths (e.g., Meier *et al.* 2010).

When using the stretching method, a theoretical formulation was introduced to estimate the error when computing *dv/v* (Weaver et al., 2011a). This estimation relies on the assumption that the correlation coefficient corresponds to a lack of convergence of the CCF toward the real GF. This lack of convergence produces an apparent stretching factor that can fluctuate statistically. The resulting root mean square (*rms)* error depends on the maximized correlation coefficient CC between the stretched and reference cross-correlations, but also on the frequency bandwidth, on the time window $[t_1, t_2]$, and on the central pulsation (Weaver et al., 2011b):

$$rms_{dv/v} = \frac{\sqrt{1-CC^2}}{2CC} \sqrt{\frac{6\sqrt{\frac{\pi}{2}}}{F\omega_c^2\left(t_2^3 - t_1^3\right)}} \quad (5)$$

Consequently, extending the frequency bandwidth or the time window duration reduces the *rms*, and a lower *CC* causes a higher *rms* error.

More empirically, the *dv/v* can be statistically computed for several configurations (e.g., multiple time windows and/or multiple sensor pairs) to extract their average, standard deviation, or probability density functions (Voisin et al., 2016). For the best possible robustness, the two approaches should be combined. In the case of arrays of several seismometers, the averaging approach increases robustness, but also reduces spatial sensitivity when locating the precursory signal. Therefore, rules for warnings should be based on multiple indicators at the same time: the average *dv/v* value, the statistical standard deviation over multiple pairs or multiple time windows, and the *rms* computed from the *CC*.

3.5 Instrumental instability

When computing velocity variations, a fixed distance must be maintained between sensors, and seismic records must be accurately timed. In some studies, seismic sensors were installed directly on the unstable slope, for continuous monitoring (Voisin et al., 2016; Bertello et al., 2018; Guillemot et al., 2020) or time-lapse surveys (Harba and Pilecki, 2017; Bertello et al., 2018). This type of installation could lead to alterations to the relative distances between sensors over time, as illustrated in Fig. 9. This design may be intentional, for practical reasons on large landslides, or unintentional if landslide boundaries are undefined or evolving. In both cases, the positions of the sensors should be verified. This effect may be neglected if the extent of the variation is small. For example, Voisin et al. (2016) measured variations in inter-sensor distance of a few centimeters and considered them negligible compared to the total inter-sensor distance of hundreds of meters, and to the *dv/v* variations measured of several percent. On Gugla rock glacier, Guillemot et al. (2020) suggested that an observed linear trend of variation in the *dv/v* could be explained by the modification of the inter-sensor distance *dl/l*, that were of the same order of magnitude (≈0.1%). Thus, in general, geometrical changes are negligible compared to seismic velocity changes.

Inaccurate time recording may also be a potential problem (Stehly et al., 2007). In general, records are synchronized by using the same digitizer for multiple sensors, or resampled after recording based on GPS time-stamp synchronization. However, GPS may not always be available, particularly on steep mountainous slopes with extensive vegetation cover (often the case on landslides), and precipitation or snow may also affect GPS reception. In case of doubt, the synchronization should be verified. Desynchronization of one sensor compared to another results in asymmetrical CCF drift, which is easily checked, and can be corrected for (Sabra et al., 2005).

In conclusion, the need to have a stable distance and synchronized timings when computing a velocity are trivial. In practice, geometrical changes or time desynchronization have not been real limitations in field experiments up to now. Nevertheless, their explicit verification on landslide studies would produce more robust results.

Fig. 9: Example of a monitoring installation on the Montevecchio earthflow, where non-negligible relative displacement of the four seismic sensors might occur. From (Bertello et al., 2018).

4 Spatiotemporal variations in the noise field

Several environmental factors may lead to spurious variations in the computed apparent velocity, such as variations in sources of ambient noise, loss of CCF correlation coefficient due to changes to scatterers in the propagation medium, and variations in resonance frequency as a result of geometrical changes to the medium. These factors could influence the CCF and therefore the apparent velocity measured, without necessarily representing a true change of velocity in the material. In our opinion, the stability of these factors should be verified to ensure that apparent velocity changes can be safely interpreted.

4.1 Coda wave decorrelation

In addition to relative seismic velocity changes (*dv/v*), another indicator can be directly measured from coda wave interferometry: the *CC*. Indeed, we can easily compute the waveform correlation between the CCFs for the reference period on the first hand, and the CCFs for the day (or hour) of interest on the second hand. When using the stretching method, *CC* computation is straightforward. It is defined as the maximized coefficient correlation between the reference signal and the stretched one, which is used to select the best stretching factor, together with its corresponding *dv/v* value (see eq. (4)). Hence, coda wave interferometry can be used to directly compare the different CCFs, and this comparison can itself be used as an additional indicator.

Also known as “coda wave decorrelation”, the CC indicator quantifies waveform changes. These changes are highly sensitive to structural and geometric changes, together with fluid injection. These types of subsurface alterations modify the location of scatterers and the wavepaths of scattered seismic waves, thus impacting the waveform of the coda part of the CCF. The decorrelation is also used as a proxy for fluid injection into the porous medium monitored. This method takes advantage of the high sensitivity of diffusive coda waves (late arrivals) to track tiny changes in the structural, geometric, and scattering properties of the medium.

The ratio between the observed wavelength and the size of the scatterers strongly affects the influence of the scatterers on the CCF. When the wavelengths are significantly larger than scatterers, the wave have small interactions with them, ballistic wave propagation dominates the CCF, and variations of the *CC* indicator may not be adequate for observing changes in the scatterers. This regime has been studied on sedimentary soils (Konstantaki et al., 2013), rocks (Winkler and Nur, 1979), and concrete (Abraham et al., 2012; Garnier et al., 2013). All these materials show variations in elastic wave velocity and attenuation with water content. But when the wavelength is of the same order of magnitude than heterogeneities of the medium, multiple scattered waves become also sensitive to variations in scattering propertiess. Therefore, changes to the scatterers and reflectors (position, or reflection coefficient), or in the attenuation of the propagating medium, would modify signals coming from the scatterers, and consequently alter the shape of the coda part of CCFs (e.g., reflection interferometry: Draganov et al., 2007; Wapenaar et al., 2010; Draganov et al., 2013).

Structural changes to the landslide’s subsurface may modify neighboring scatterers and reflectors, consequently decreasing *CC* over time. Coda wave decorrelation has been used as an indicator of deconsolidation in a few landslide studies (Fiolleau et al., 2020; Guillemot et al., 2020), with the depth of the deconsolidation estimated from the frequency range studied. The depth can also be estimated from the time-window of the Green's function after which decorrelation is observed (Planès et al., 2015), based on the body-wave sensitivity kernel. This technique might be applicable on deep landslides with considerable heterogeneity and rapid kinematics.

Water pore filling in a porous medium also changes scattering wavepaths, leading to a decrease in *CC*. In fact, Thery et al. (2019) performed laboratory experiments to monitor water level elevation in sand and water infiltration in concrete. Using active ultrasonic waves, they measured the *CC* in the coda using the stretching method, and then defined the decorrelation value $Kd = 1 - CC$. Results from both experiments indicated that Kd is more sensitive to water than the apparent velocity change *dv/v*. When applied in a geophysical context involv-

ing fluid infiltration into porous media, this method provides new insight and perspectives for volcanoes, landslides and rock glaciers monitoring (Thery et al., 2019). Indeed, a drop in *CC* has been observed on partially frozen porous media like rock glaciers during melting periods, reflecting percolation of liquid water within the surveyed medium (Guillemot et al., 2020). Hence, the *CC* indicator helps to track noise instabilities induced by the presence of water, which is a major source of scattering changes.

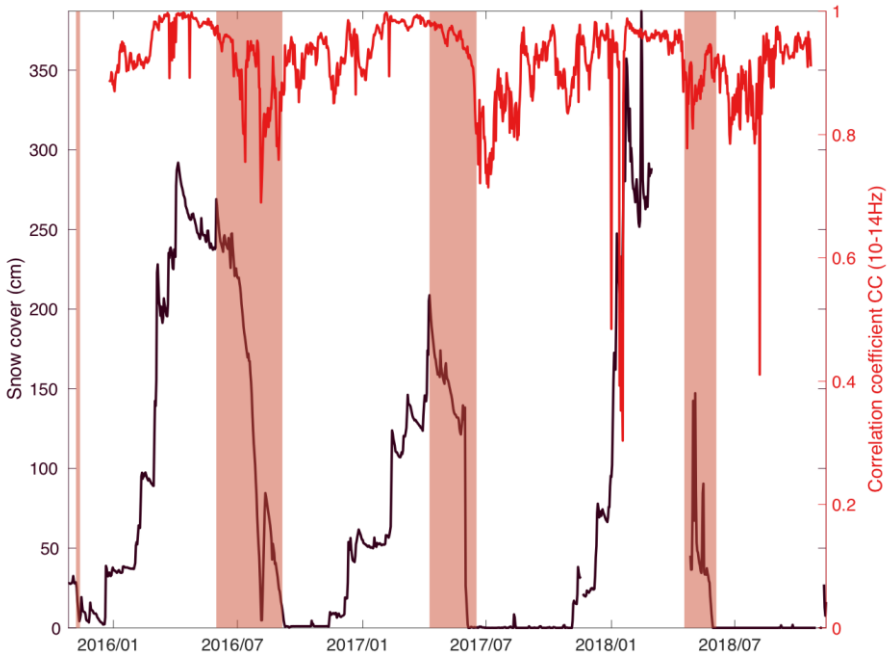

Fig. 10: Correlation coefficient *CC* (red) between a stretched and a reference signal, computed for the Gugla rock glacier using the stretching method in the 10–14 Hz frequency range. Snow-cover measurements (black) were taken at the same location. Red boxes highlight the main melting periods over the three years. The *CC* dropped as melt water percolated into the medium (Guillemot et al., 2020).

Another outcome of coda wave decorrelation is related to the processing strategy. Indeed, monitoring of the apparent velocity—which requires stable scatterers—may become biased as a result of a low *CC* caused by a modification of the CCF shape (cf eq. (4)). This low CC may result in large uncertainties on the computed *dv/v* (cf. eq. (5)) (Weaver et al., 2011b). Therefore, it is worth computing the *CC* together with *dv/v*, to estimate its degree of confidence. At a low *CC*, the *dv/v* indicator is no longer reliable, and changes in the medium should be observed only based on the *CC* indicator. When the CCF evolves significantly along time, the *CC* can be improved by using an adaptative reference CCF (see 3.3.4).

4.2 Sources of ambient noise

Identifying seismic noise sources is a key challenge to be undertaken before computing the CCFs, as variations in the sources may influence the resulting apparent *dv/v*. Indeed, sources of seismic noise vary across space, time, and frequency bands (Peterson, 1993; Bonnefoy-Claudet et al., 2006; McNamara and Boaz, 2019). Landslide monitoring mostly uses noise

within 1−20 Hz spectra (Fig. 14), where at least 50% of the noise is anthropogenic, i.e., produced by human activities such as vehicle traffic, machinery, factories, and wind turbines (e.g., Planès et al., 2017; Lecocq et al., 2020). Anthropogenic noise often displays daily and weekly cyclic variations, due to reduced human activity at night and on weekends (Bonnefoy-Claudet et al., 2006; McNamara and Buland, 2004). Anthropogenic noise also varies in space, and is lower for example in rural or desert areas than in urbanized spaces. Additional ambient noise is also produced by regular natural sources such as wind turbulence around topographical irregularities (McNamara and Buland, 2004; Young et al., n.d.), the coupling of tree motion to the ground through their roots (McNamara and Buland, 2004; Withers et al., 1996), local surf in the sea, and glacier displacement and melting (Gimbert et al., 2016; Preiswerk and Walter, 2018). The distribution of these sources of noise across space promotes a more homogeneous noise field, which can be useful to obtain more stable CCFs. Finally, landslides themselves (Suriñach et al., 2005; Provost et al., 2018b), or events such as snow avalanches (van Herwijnen and Schweizer, 2011; Lacroix et al., 2012), can also generate noise above 1 Hz due to friction within the material, thus creating instability within the ambient noise. It should be noted that natural noise may also vary seasonally or daily due to environmental forcings.

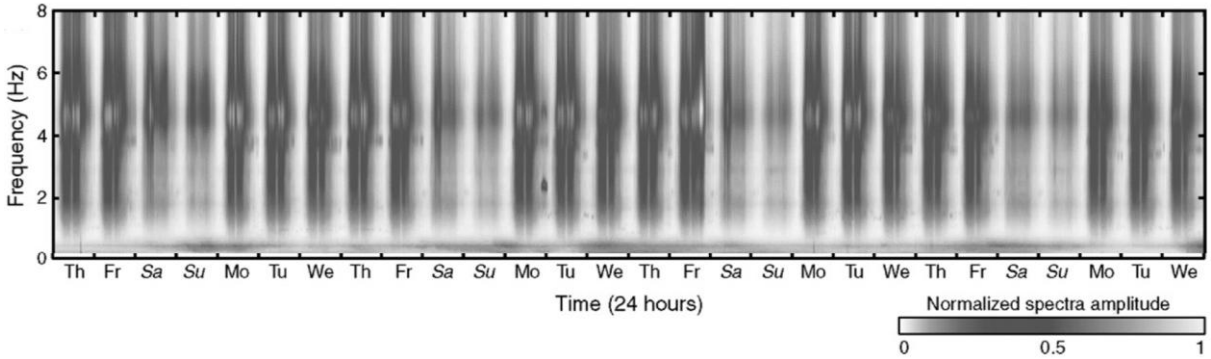

Fig. 11: "Normalized Fourier spectra amplitude recorded in an urban area (Grenoble, French Alps) from 10.06.2004 to 22.07.2004", vertical component. At frequencies > 1 Hz, the noise displays daily and weekly fluctuations, due to anthropogenic activity. From (Bonnefoy-Claudet et al., 2006).

These fluctuations of the sources might make it difficult to accurately reconstruct the Green's function for *dv/v* computation (Hadziioannou et al., 2009). Indeed, as well as reducing the *CC*, a variation in the frequency content or in the location of the sources (=source anisotropy) could alter the apparent *dv/v*, regardless of the physical changes occurring in the propagation medium tested (Zhan et al., 2013; Froment et al., 2010). For example, water released as snow melts on a glacier can induce daily noise amplitude peaks, and alter the apparent *dv/v* by changing the direction of the energy flux (Preiswerk and Walter, 2018). On a petroleum platform, Delaney et al. (2017), recorded *dv/v* fluctuations of 0.25% at [0.55-1.55] Hz, and attributed them to variations in the mean noise source azimuth (≈ 90°) that oc-

curred between two consecutive days. On Los Angeles Basin, Zhan et al. (2013) suggested that the previously observed seasonal velocity variation of 0.05% (at f <0.5 Hz) (Meier et al., 2010), could be caused by differences in the wave field frequency content between winter and summer, rather than by true variations in the velocity of the bulk. At higher frequencies, Mikesell et al. (2015) modeled the variation in frequency content of a source using the stretching method between a 14-Hz source wavelet and a 16-Hz wavelet. At these higher frequencies, they found variations of less than 0.1%, caused by changes in the frequency content. Overall, these instabilities of apparent velocity variations appear to remain relatively small, or in any case smaller than the precursor signals before landslide destabilization, which corresponds to several %. Therefore, coda wave interferometry may be suitable for use in landslide early-warning applications. In addition, anthropological noise often comes from cities, roads, and rivers, that are stable in space, and if averaged over a few hours or more, can be considered stable in time (Delaney et al., 2017; Voisin et al., 2016). This stability holds true as long as no new local sources (roads, engines, or factories) are installed close to the landslide.

To avoid spurious fluctuations caused by an unstable source, the stability of sources over time and space within the frequency studied can be investigated. The anisotropy of the sources and its fluctuation over time can be measured with a network of sensors by using microseimic methods, or by measuring the asymmetry of the cross-correlations (Renalier et al., 2010b; Stehly et al., 2006). Unstable source location can be corrected for by discriminating between noise sources in the time domain and computing separate CCFs for each source category (e.g., traffic or no traffic on a road) (e.g., Planès et al., 2017). Spatially-inhomogeneous sources may be homogenized using the C3 method with a network of sensors, where each sensor is considered as a virtual source (Stehly et al., 2008). Alternatively, the influence of unstable noise frequency content on the *dv/v* can also be reduced by whitening the coda of the correlation—instead of the traces only—(Daskalakis et al., 2016), or by estimating and accounting for the error caused by the noise source variations (Delaney et al., 2017). Finally, the influence of unstable sources can be mitigated by comparing CCFs measured inside and outside the landslide, placing the pairs of sensors far enough apart to have clearly separate sensitivity kernels.

4.3 Resonance frequency

Some sites, such as rock columns, may exhibit resonant frequencies and polarization (Nakamura, 1989) that vary over time, often under the influence of environmental factors such as ground temperature (Bottelin et al., 2013a, 2013b, 2017; Colombero et al., 2018; Valentin et al., 2017). The resonance frequency of a zone depends on the mechanical charac-

teristics of the material (v_p, v_s, density), but also on its geometrical features (size and shape of the object).

A change in resonant frequency would alter the apparent velocity. Indeed, the traces recorded between two sensors should be more coherent at the resonance frequency. This remains true even after frequency-normalization—or whitening—presented in section 3.1. As a result, the CCF spectra becomes dominated by the resonance frequency, which we can write as

$$CCF_1(t) = A(t) \times \cos(2\pi ft) + r(t) \quad (6)$$

Where *A(t)* is the amplitude of the resonating oscillation over time and *r(t)* the residual component of the CCF that is not due to the resonant frequency. A change in the resonance frequency by a factor ε would change the CCF as follows:

$$CCF_2(t) = A(t) \times \cos(2\pi f(1+\varepsilon)t) + r(t) \quad (7)$$

Considering $r(t)$ small enough compared to *A(t)*, a change in resonant frequency would lead to a change in apparent velocity that is equivalent to stretching the time *t*, as in equation (4). If the change in resonant frequency is caused by a change in seismic velocity, the resulting *dv/v* alteration would correspond to a true change occurring in the bulk material. However, if the change to resonant frequency is caused by a change in geometrical features, the apparent *dv/v* variation should be rather interpreted as a change in local geometry (also useful information), with no change to the seismic velocity of the material. In this case, it may be more appropriate and accurate to directly measure the resonant frequency rather than using the *dv/v*. We suggest that this effect explains the strong correlation between the time series of *dv/v* and resonance frequencies (H/V method) reported by Colombero et al. (2018) for a prone-to-failure rock compartment (Fig. 12). In their study, the relative variation in velocity and resonance frequency both fluctuated seasonally within 20% peak-to-peak. The influence of resonance frequency could explain why this seasonal *dv/v* amplitude, observed at 2–4 Hz, was far outside the trend displayed in Fig. 14. Note that the *CC* was highest at the resonance frequency, showing that care should be taken when using the *CC* as the only quality indicator of the *dv/v* result (Weaver et al., 2011b). Finally, a sensor placed near the resonating structure might also be affected by the resonant frequency, due to irradiation by the structure of ambient noise dominated by its resonant frequency. If this is the case, the resonating structure should be considered to be an unstable secondary source of ambient noise (see 4.1).

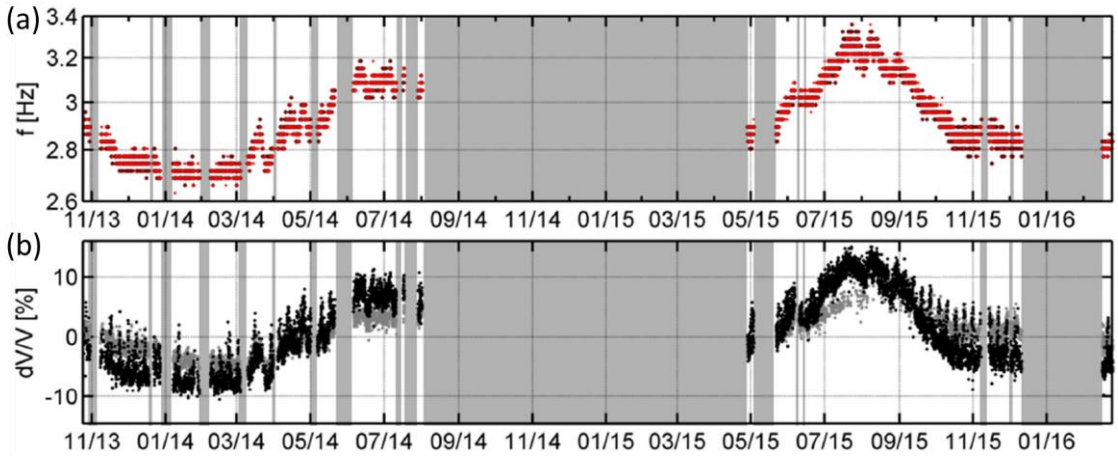

Fig. 12: Time series showing (a) the resonance frequency of the Madonna del Sasso rock column computed by H/V, between October 2013 and February 2016. (b) Apparent *dv/v* obtained from cross-correlation of the horizontal component (North in black, South in gray) from a sensor placed on the rock column and a sensor placed outside, at 2−4 Hz. The two curves are highly correlated, showing a relative peak-to-peak amplitude of 20% (Colombero et al., 2018)

Variations of *dv/v* within the band of a strong resonance frequency should therefore be interpreted with care. When possible, the stability and amplitude of the resonance frequencies should be verified directly using the horizontal-to-vertical spectral ratio method (H/V) (Nakamura, 1989). Any resonance frequency may simply be eliminated by applying an appropriate frequency filtering to the traces or the CCFs, or attenuated by equalizing the frequency content of the CCFs (Daskalakis et al., 2016).

5 Environmental influences on the apparent velocity

5.1 Seasonal fluctuations

Seasonal fluctuations in *dv/v* were clearly observed on the shallow and deep-seated landslides at Pont-Bourquin (Fig. 13) and Utiku, respectively (Larose et al., 2015; Bièvre et al., 2018; Voisin et al., 2016). These fluctuations were suggested to be caused by yearly cycles of environmental factors, such as soil temperature and precipitations. Understanding and predicting these seasonal variations are necessary to distinguish them from possible precursory signals. However, few studies of seasonal variations have been performed on soft-soil landslides, and to better understand seasonal effects, the scope of the present review must be extended to non-landslide investigations.

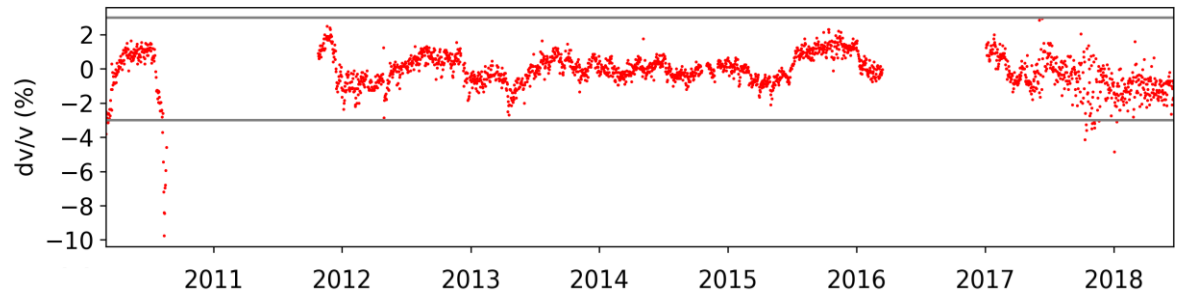

Fig. 13: (a) Relative daily velocity changes *dv/v* at Pont-Bourquin landslide between March 2010 and June 2018, computed by stretching at frequencies of 10–14 Hz, with a ±[0.2,0.6]-s time window. The horizontal gray lines in the *dv/v* represent a possible threshold of ±3%. The 2010 drop and the seasonal amplitude are slightly higher here than reported in previous studies (Mainsant et al., 2012b; Larose et al., 2015; Bièvre et al., 2018) because the 10–12 Hz frequency signal was used.

$\Delta v/v_{max} \sim f^{3/2}$

Seasonal variations in *dv/v* have also been observed at non-landslide sites, including volcanoes, sedimentary basins, groundwater storage, CO_2 storage, glaciers and ice sheets, and even lunar soil (Table 2). A first glance at the corresponding data reveals that the amplitude of seasonal variations varies by a factor of 200 between studies, from 0.03% (Lecocq et al., 2017; Wang et al., 2008) to 6% (James et al., 2017). This extensive range is mostly explained by the different frequency ranges and subsequent investigation depths considered. Indeed, when comparing the studies to each other, the seasonal amplitude appears to be linked to the central frequency f chosen to filter the CCFs (Fig. 14). The trend provides a good fit for the data from all the study sites. There are only two outliers, on the Moon (Sens-Schönfelder and Larose, 2008) and on Greenland's ice sheet (Mordret et al., 2016), which are special case studies. Since higher-frequency surface waves are sensitive at shallower depths, the observed trend confirms that near-surface soil is more sensitive to seasonal variations than deep material. Inter-station distances and time windows also follow a trend with the seasonal amplitude-variations (not shown here): in practice, these parameters are also linked to the investigation depth. In fact, multiple studies report an increase in seasonal variations with early time windows (Sens-Schönfelder and Wegler, 2006; Richter et al., 2014; Hillers et al., 2015b), shorter inter-station distance (Meier et al., 2010), and higher frequencies (Richter et al., 2014; Voisin et al., 2016). Only one study reported a decrease in seasonal variation when the frequency was increased (Hillers et al., 2015a), and this effect was explained by the sensitivity of deep rocks to thermoelastic strain.

Two conclusions emerge from this trend. First, the consistency of the trend observed across several regions and for different materials demonstrate a consistent behavior between landslides and other sites for the seasonal variations. Secondly, seasonal *dv/v* variations should be greater when monitoring shallow landslides than deep-seated landslide, due to the difference in frequency filtering. Indeed, the surface-wave sensitivity depth estimated in the publications reviewed here was roughly of the order of 10 m at 10 Hz, hundreds of meters at 1 Hz, and

kilometers at 0.1 Hz. The landslides studied, with a depth ranging from 2 m to 300 m, were observed within the 1.3–20 Hz range. In most cases, seasonal variations were small compared to the velocity drops observed before or during a failure.

Study	Frequency (Hz)	Amplitude (%)	Context	Suggested governing influence (correlation sign, lag time)
Sens-Schönfelder and Wegler (2006)	Broadband>0.5	4	Volcano, Merapi, Indonesia	Groundwater level (–)
Sens-Schönfelder and Larose (2008)	6–11	0.15	Lunar soil, Apollo 17	Temperature (+, 7 d)
Meier et al. (2010); Tsai (2011)	0.1–2	0.1	Basin, Los Angeles, USA	Groundwater level (–)
	6–8	2.2		
Voisin et al. (2016)			Landslide, Utiku	Groundwater level (–)
	3–20	6		
Bièvre et al. (2018); Larose et al. (2015)	8–12	3	Landslide, Pont-Bourquin, Switzerland	Rainfall (–), temperature (+, 40 d), frost (+)
Wang et al. (2017)	0.15-0.9	0.03	Whole Japan, Hi-net	Pore pressure (–), snow depth (+), sea level/tide (+), *Temperature (+, 40 d)*
Miao et al. (2018)	Broadband <30	*0.3 ms*	East Japan, Kik-net	Rainfall (–)

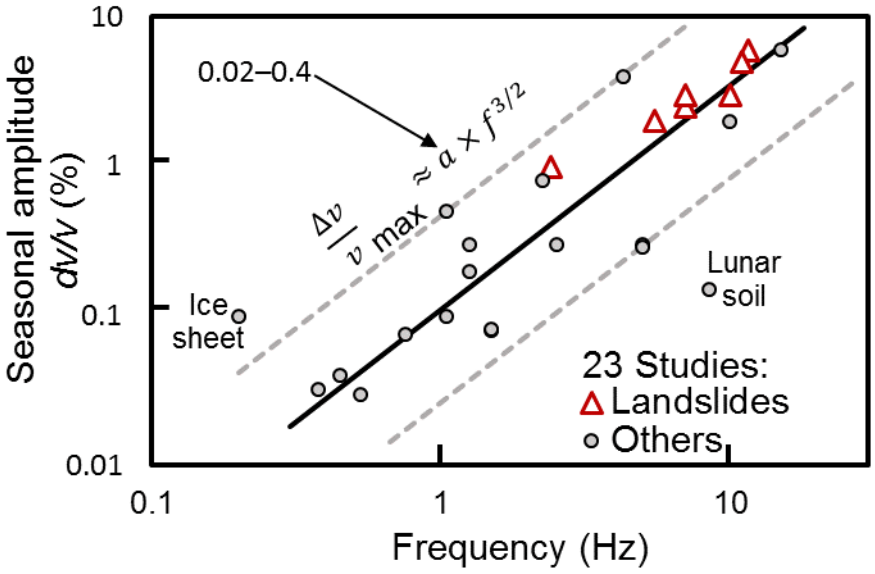

Fig. 14: Amplitude of seasonal variations in relative velocity, versus central frequency. Coefficient a = 0.11 (dashed lines: 0.025 and 0.45). Landslides also include Gugla rock glacier.

5.2 Fluctuations occuring within a day

Improving the time resolution down to a few hours would greatly improve the lead time for the *dv/v* method, but requires to handle daily cyclic fluctuation of apparent velocity. The velocity fluctuations occurring within daily cycles has not been studied on landslides, but a small number of studies on non-landslides can provide insights on these fluctuations (see Table 3). Daily fluctuations have been little studied on deep geological structures, because the small dv/v variations of deep structures require a high measurement accuracy (typically $<10^{-3}$, see Fig. 15) that requires stacking the CCFs over one day or more to improve their signal-to-noise ratio. Furthermore, the inertia of deep structure reduces the interest of observing them at a sub-daily resolution. In contrast, the observation of shallow layers is likely to reveal stronger *dv/v* variations (several %) and to tolerate a lower signal-to-noise ratio.

Observing daily fluctuations of dv/v is challenging: the low stacking time reduces the signal-to-noise ratio, and the daily fluctuations in the sources may introduce spurious velocity variations that do not reflect changes in the medium (discussed in 4.1). To handle these difficulties, it is necessary to adapt the processing workflow. However, no standard technique has yet emerged for studying daily fluctuations in *dv/v*. Thus, for example, Takano et al. (2014) computed CCFs every minute between 2 a.m. and 4 p.m., then averaged periods of tidal dilatation and contraction separately over three months. Alternatively, Planès et al. (2017) and Voisin et al. (2017) used the energetic early arrivals of the CCFs after verifying the stability and azimuth of the source, and discarding unstable sources. In contrast, Mao et al. (2019) denoised the correlation by applying a Wiener filter (Moreau et al., 2017) and averaged the *dv/v* over 1225 pairs from a seismic sensor network. And finally, Richter et al. (2014) com-

puted a *dv/v* between each hourly correlation and their average calculated for the same day, then computed the averaged *dv/v* over 1570 days, for each hour of the day, after discarding the values associated with a low *CC*.

Table 3: Variations in *dv/v* occuring within a day that were reported in the literature.

Study	Frequency (Hz)	Amplitude of dv/v (%)	Context	Suggested governing influence
Takano et al. (2014)	1–2	0.19	Volcano, Iwate, Japan	Tidal strain (velocity decrease during dilatational episodes)
Takano et al. (2019)	2−4	0.6	Volcano, Izu-Oshima, Japan	
(Hillers et al., 2015c)	2−8	0.6	Piñon Flat Observatory, California.	Tidal strain
James et al. (2017a)	13–17	0.2	Permafrost, Poker Flat Research Range, Alaska	No suggestion for daily variations (only seasonal)
Planès et al. (2017a)	5–20	5	Sea levee, Colijnsplaat, Netherlands	Pore water pressure (–) [due to sea tide levels]
Joubert et al. (2018)	7−13	5	Sea dike	Sea tide level (–)
Preiswerk and Walter, (2018)	4–16	*CC drop*	Glacier, Plaine Morte, Switzerland	Source variation, due to drainage/filling of a glacier-dammed lake
Mao et al. (2019)	1–5	0.02	Volcano, Piton de la Fournaise, La Réunion	Tidal strain, temperature
Voisin et al. (2017)	5–12	3	Groundwater storage, Crépieux-Charmy, France	Groundwater levels (–) controlled by fluid injection
Richter et al. (2014a)	4–6	0.09	Northern Chile	Temperature (+, with a lag)

The reviewed literature shows that the seismic velocity in the first meters of soil may vary rapidly throughout the day. Daily cyclic variations of *dv/v* have been observed, and attributed to thermally induced stress (Richter et al., 2014; Mao et al., 2019). In many areas, a daily cycle of *dv/v* might also be caused by variations of the anthropogenic noise (see 4.2). Additionaly, cycles of half days were also observed, and attributed to earth tide stress (Takano et al., 2014; Mao et al., 2019), or to marine tide that induces a groundwater level changes near the sea (Planès et al., 2017). A better understanding of the environmental influences on the fluctuations of *dv/v* (temperature, rainfall, frost, tide, or simply source variations) would help to distinguish them from a potential precursor, which is the aim of the next section

5.3 Reversible environmental factors

Correlations observed between the *dv/v* and environmental factors suggest an influence of several factors on the *dv/v* (detailed in section 5.3), such as groundwater level, shallow soil temperature, soil freezing/thawing, snowfall or tide.The studies are consistent on the follwing governing factors. A higher groundwater elevation decreases the apparent velocity. Higher temperature increases it (if T>0 °C) with several days of lag. In cold conditions, soil freezing increases the velocity, whereas soil thawing decreases it.

Some governing causes suggested in the studies listed in Table 2 may also appear unclear. For example, temperature and groundwater levels are often mentioned, but are difficult to discriminate between because they are often mutually correlated over the year. Furthermore, several of these phenomena may differ spatially from one region to another (Wang et al., 2017), consequently their influences must be studied locally. Their amplitude can be reduced empirically using a linear model based on the influence factors measured (pore pressure changes, sea level, air temperature, snow height) that is fitted empirically to the raw *dv/v* time series for each region. Subtracting this empirical model from the raw time series then helps to distinguish events of interest from seasonal fluctuations (e.g., Wang et al., 2017). Yet, to handle these influences more accurately, the processes causing the fluctuations must be better understood. Such understanding will require further investigations, with in-situ monitoring of the adequate environmental parameters, that are highlighted.

5.3.1 Groundwater

A better understanding of the influence of groundwater is essential when studying rainfall-induced landslides, to discriminate *dv/v* drop due to normal groundwater elevation (e.g., Fig. 16) from *dv/v* drop due to soil liquefaction preceding a failure (Mainsant et al., 2012b). The phenomena should be studied at the time scale of a few days for early warning. On the Utiku landslide, Voisin et al. (2016a) reported a clear negative correlation between the water table level and the *dv/v* (Fig. 15.a). Similarly, on the Pont-Bourquin landslide, cross-correlation between *dv/v* and rainfall over four years revealed a clear peak of negative correlations, with a lag of 2–5 days explained by the delayed water infiltration (Bièvre et al., 2018) (Fig. 15.b).

Precipitations, and the resulting increase in groundwater levels, were rapidly suggested to decrease the apparent *dv/v* over a time scale of months (Sens-Schönfelder and Wegler, 2006). Indeed, over a 15-year observation period, Clements and Denolle (2018) found the *dv/v* to reflect changes in regional groundwater levels, marked by long depletion and rapid replenishment as a result of a succession of droughts and floods. At a sub-daily scale, Planès et al. (2017) reported a negative correlation between *dv/v* and pore water pressure, generated by the tides under a sea levee, with a 12 hours cycle (Fig. 17) (see 5.3.5). Finally, a negative correlation between groundwater levels and *dv/v* within a time frame of hours to days was also confirmed in a controlled fluid-injection experiment (Voisin et al., 2017).

Groundwater levels could influence the *dv/v* through two mechanisms: poroelasticity and direct water loading. In the poroelastic mechanism, the water filling open pore spaces would increase the homogenized bulk modulus and the averaged density of the soil, therefore altering the seismic wave velocity (Grêt et al., 2006a). According to this mechanism, groundwater

would both increase the P-wave velocity and decrease the S-wave velocity. This would result in a clear decrease in surface wave velocities (Biot, 1962) which are mostly (90%) sensitive to S-waves velocity (Grêt et al., 2006b). This direct poroelastic effect mainly affects the shallow layers where the water table fluctuates (Meier et al., 2010; Hillers et al., 2014). The second mechanism, direct water loading, may have two contrasting effects depending on the wave's sensitivity depth (i.e., related to the frequencies studied). Near the surface and in confined layers, the load of the water mass will increase pore pressure (Voisin et al., 2017; Wang et al., 2017; Clements and Denolle, 2018). Indeed, if the area cannot drain, pore pressure leads to cracks opening and decreases the area of grains in contact, hence decreasing the seismic velocity (Rivet et al., 2015). At deeper layers, under the groundwater table or under impermeable layers, the water load will increase the stress on the granular matrix, increasing the seismic velocity (Obermann et al., 2014).

In conclusion, precipitations and rising groundwater levels decrease the surface wave velocity, and therefore the *dv/v*, on shallow landslides. Correcting the effect of groundwater levels on the *dv/v* would require an indication of groundwater levels fluctuations, estimated from precipitations (e.g., Sens-Schönfelder and Wegler, 2006) or measured directly at depth (e.g., Voisin et al., 2016). Because unstable slopes hydrological processes are heterogeneous in time and space (Brönnimann, 2011), several in situ measurements would ideally be required.

As a side application to providing precursors to failure, the *dv/v* method could be used to non-destructively estimate groundwater levels on a landslide (Voisin et al., 2017, 2016). This usage would complement piezometric measurements which are difficult to maintain over long periods on a moving landslide and only provide local measurements. However, estimating groundwater fluctuations using the *dv/v* (Clements and Denolle, 2018) might require to distinguish it from other influence factors, such as the thermoelastic effects that might influence the *dv/v* to a similar extent (see next section).

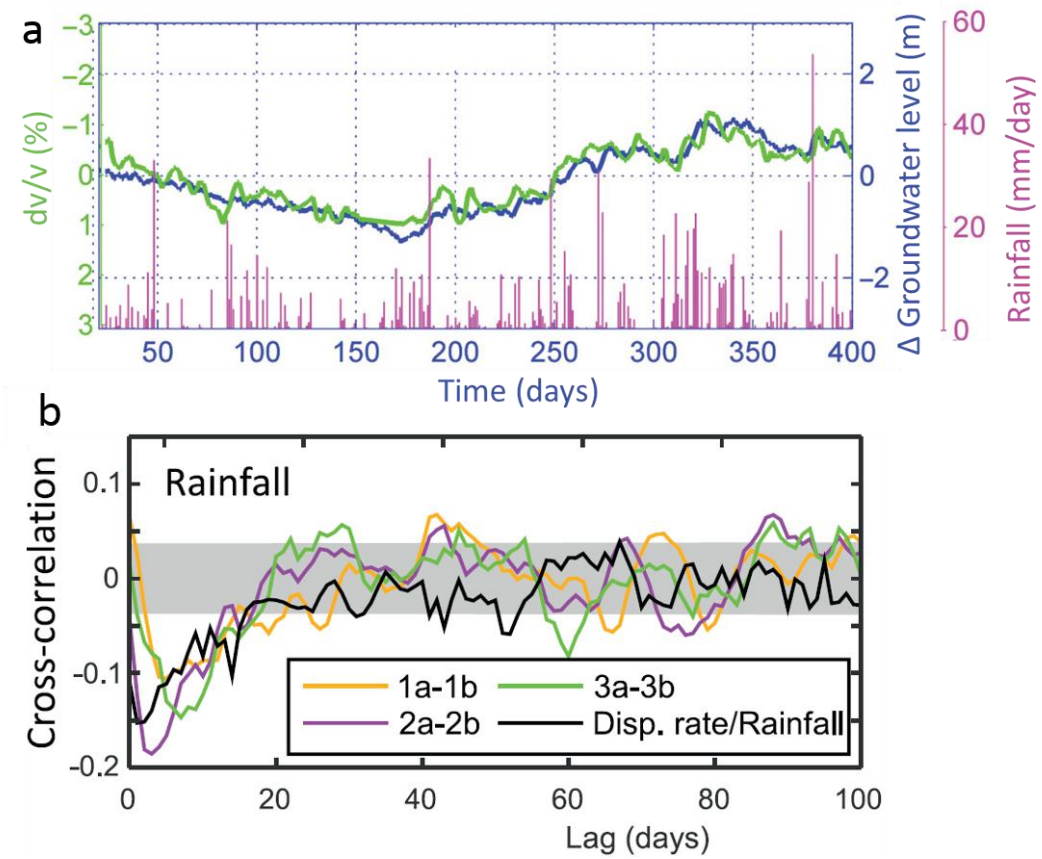

Fig. 15: Influence of water on two landslides. (a) On the Utiku landslide, measurements of dv/v (inverted axis) over a year show a clear negative correlation between dv/v and groundwater levels measured—from (Voisin et al., 2016). (b) On the Pont-Bourquin landslide, the cross-correlation between dv/v and rainfall (colored curves represent three pairs of sensors) over four years shows a clear peak of negative correlations 2–5 days after the rainfall event, due to the infiltration delay. A shorter delay was observed between rainfall and displacement rate (in black)—from (Bièvre et al., 2018).

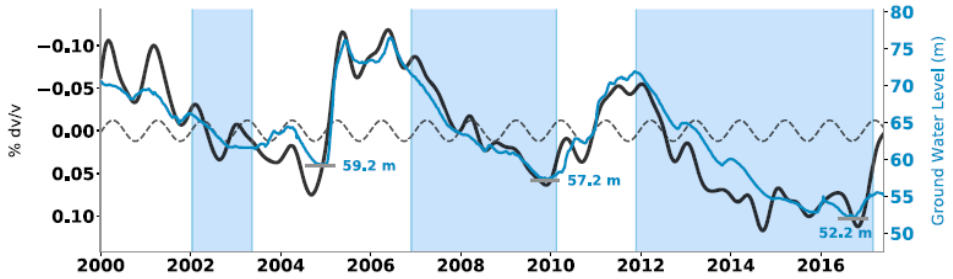

Fig. 16: How temporal perturbations of seismic wave velocity (black curve) relate to groundwater levels (blue curve) and modeled thermoelastic strain (dashed curve) in the Baldwin Park Key Well, in California Basin. From (Clements and Denolle, 2018)

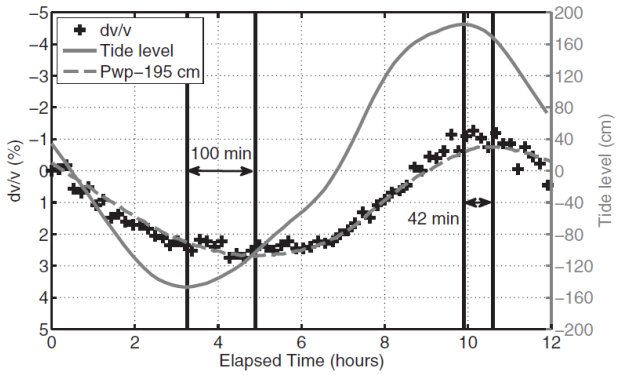

Fig. 17: On a coastal levee, *dv/v* correlates with tide level, and measurements of the groundwater level (Pwp). Groundwater level is shifted by -195 cm to superimpose with the *dv/v*. From (Planès et al., 2017)

5.3.2 Thermoelasticity

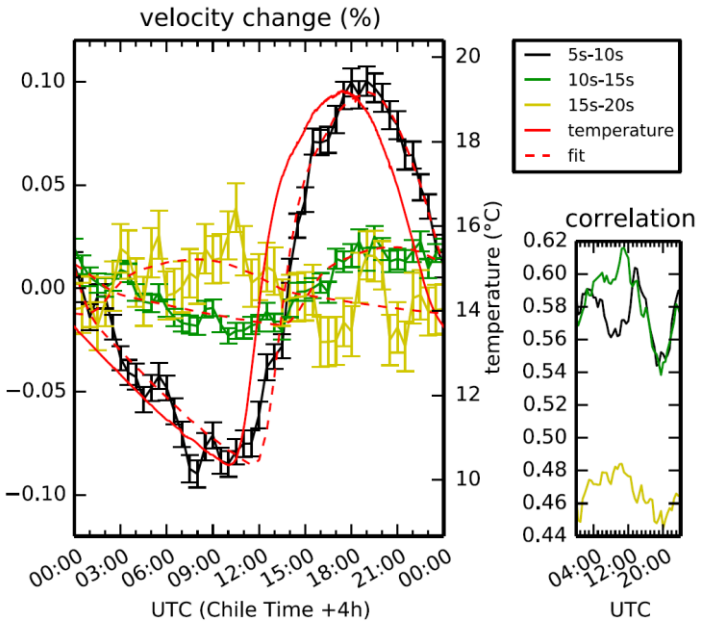

Fig. 18: Daily fluctuations in velocity and correlation coefficient at a frequency range of 4–6 Hz for three time windows, along with the air temperature, measured on dry rocky ground in the Atacama Desert. The apparent fluctuations in velocity appear to correlate well with air temperature, with a delay of 1.5 h for the 5–10-s time window. The fitted curves represent the temperature curve, scaled and shifted to mirror the *dv/v* data. From (Richter et al., 2014)

In many studies, air temperature is reported to correlate positively with the *dv/v*, with a time lag (e.g., Hillers et al., 2015; Lecocq et al., 2017). This correlation was observed at a seasonal scale on the Pont-Bourquin landslide, with a ≈30-day lag (Bièvre et al., 2018), suggesting that the temperature might control the material's rigidity, through soil moistening or drying. The 30-day lag would locate the sensitivity of *dv/v* in the shallow layer (2 m or less), according to 1D heat wave diffusion modeling (Bièvre et al., 2018). However, other parameters such as groundwater levels, or snowfall and subsequent melting, also often correlate with temperature over a year, making them hard to discriminate at a seasonal scale. The influence of tempera-

ture was distinguished from that of groundwater in Richter et al. (2014) (Fig. 7) and Sens-Schönfelder and Larose (2008), as the respective measurements for these studies were taken in an arid desert and on the moon without water. Hillers et al. (2015a) suggests thermoelasticity to mostly control *dv/v* seasonal variations (±0.2% at 0.5 − 2 Hz) observed for 4 years at the San Jacinto fault area: the correlation and the lag with the *dv/v* better matched a thermoelastic model than other potential mechanisms (wind speed, source variation, rainfall, groundwater levels, atmospheric pressure).

Modeling the thermal influence on stresses can help to estimate the amplitudes and time lags of *dv/v* in order to discriminate thermal effect from other effects. Two configurations, with freely expandable or confined medium, are considered. If the material can expand freely at the surface, and assuming a constant pressure, rigidity will decrease with temperature. In such configuration, *dv/v* would be negatively correlated with temperature (Anderson et al., 1968), which is contradictory with most of observations (Table 2). However, in a confined medium that cannot expand freely, stress increases with temperature, increasing the seismic velocities at depth. A higher stress then increases the *dv/v* (Larose and Hall, 2009). In this configuration, the thermally induced stress is a plausible explanation for the positive correlation observed between temperature and *dv/v* (Tsai, 2011; Richter et al., 2014).

To explain the lag time of thermally induced stress, the diffusion of temperature at depth must be modeled. Temperature fluctuations propagate with a depth-dependent lag through heat conduction waves. Considering a 2-D elastic half-space in plane strain, and a 1-year or 1-day periodic thermal forcing at the surface as boundary conditions, the associated strain and stress changes can be computed using a thermally constrained equation (Berger, 1975). The local velocity changes at depth are then computed using third-order (Murnaghan) elastic constants (Tsai, 2011). Finally, the *dv/v* is determined by integrating the different velocities at depth, using autocorrelation sensitivity kernels (Tsai, 2011). To improve the fitting with observations (amplitudes and lag times between *dv/v* and temperature), an unconsolidated layer may be added at the surface of this 2-D model (Ben-Zion &Leary, 1986, Tsai 2011). It is worth noticing that poorly constrained parameters and large uncertainties due to potential heterogeneity of the medium make the accuracy of these thermoelastic models not definitive (Tsai, 2011). Furthermore, the contribution of thermoelastic effect would be site dependent (Wang et al., 2017), and indeed this effect is supposed to be either major or negligible depending on the studies. Our conclusion is that thermoelastic effect indeed influences the *dv/v*. This effect should be negligible on unconsolidated materials, and play a more important role on soils and rocky materials.

Removing thermoelastic effect from *dv/v* measurements should be easier in regions where the temperature is positive all the year. Monitoring the groundwater levels and underground temperature should help to discriminate these two remaining factors. However, in colder regions such as in mountains (e.g., Bièvre et al., 2018), the *d/v* is also influenced by snow cover, snow melting or soil thawing/freezing (see 5.3.3 and 5.3.4). These factors are mutually correlated—but non-linear—with air temperature over a year, therefore discriminating them from thermoelastic effect should be made with care.

5.3.3 Soil freezing and thawing

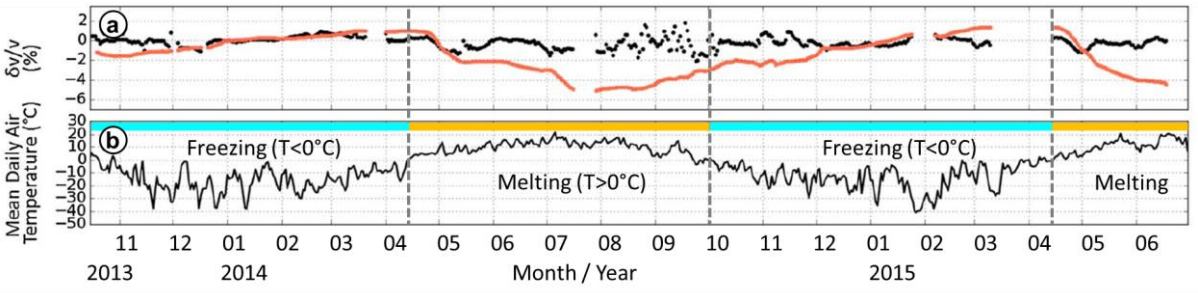

Fig. 19: Variations in (a) apparent seismic velocity computed with a fixed reference (black) and a moving window reference (red), from 2013/10 to 2015/07, on the Poker Flat Research Range, Alaska. (b) Air temperature measurements. The permafrost may melt when air temperature >0 °C and freeze when <0 °C. (James et al., 2017)

In polar and mountainous regions, several types of permafrost have been monitored by passive seismology methods, including sites subject to possible destabilization due to global warming (Gariano and Guzzetti, 2016). On Pont-Bourquin mountainous landslide, cold in winter correlated with rapid increases in dv/v, which was suggested to be caused by soil freezing (Bièvre et al., 2018). James et al. (2017) investigated discontinuous permafrost composed of frozen loess and alluvial deposits. They used coda wave interferometry to demonstrate that seasonal changes in physical properties (water-ice ratio within the active layer) can be monitored using this technique (Fig. 19). Another example of seismological monitoring of permafrost (Guillemot et al., 2020) investigated the Gugla rock glacier (Switzerland) over more than three years. Since active rock glaciers move downslope at rates between cm/yr and several m/yr, they can be assimilated to rocky landslides. Monitoring the *dv/v* reveals seasonal variations in amplitude of around 2% at $4 - 8$ Hz. This variations correlates negatively with air temperature, with a lag of around 1 month (which corresponds to the propagation of the thermal waves throughout the entire active layer, diffusing to around 5 m depth). This observation suggests that a freeze-thawing process takes place within the shallow layers.

Through this seasonal freeze-thawing cycle induced by thermal forcing and propagating at depth, the mix of coarse blocks, fine matrices, air, liquid water, and ice evolves throughout the year. Modeling shows a higher seismic velocity in winter, due to the increase in overall

rigidity of the shallow frozen layers; in contrast, seismic velocity is lower in summer as a result of the lower rigidity due to soil thawing combined with water percolation resulting from snowmelt (Guillemot et al., 2020).

A similar evolution was observed on a geological CO_2-storage site which is subject to freezing (Gassenmeier et al., 2015a). When the maximal daily temperature decreases below 0 °C, the upper part of the soil freezes, inducing a sharp increase in seismic velocity. Conversely, a drastic decrease in this velocity is observed when the soil thaws. Such variations are interpreted as the consequence of strong variations in the shear modulus between frozen and thawed soils. Quantitatively, this correlation between *dv/v* and freezing processes can be corrected by applying an empirical temperature-dependent model. In a frozen soil in Japan, the cumulative negative temperature at freezing days was found to be an indicator of the frost depth, whereas the current temperature acts as a proxy for the extent of freezing (Miao et al., 2019).

Soil freezing-thawing should be taken into account in cold and mountainous regions. Removing this effect from the *dv/v* would require an estimation of the freezing depth. Freezing depth should be estimated ideally from underground temperature measurements, or alternatively modeled from data such as precipitation, air temperature and snow depth measurements (Rankinen et al., 2004).

5.3.4 Snow

When located in polar or temperate mountainous regions, landslides are regularly subject to snow and ice cover during cold periods. The presence of this layer may have significant local influence on the mechanical, hydrological, and thermal context of the site.

Several studies mentioned a significant correlation between the presence of snow cover and measured seismic surface wave velocities. For example, changes occurring in the deep crust (around 3 to 10 km) in Greenland correlate with the ice sheet's mass balance, with a lag of 2–3 months (Mordret et al., 2016). Similarly, positive anomalies in seismic velocity are mainly controlled by snow cover in western Hokkaido, Japan (Wang et al., 2017). In shallower subsurfaces in the vicinity of Mount St. Helens volcano, a similar positive relationship between *dv/v* and snow depth was reported, with nearly zero lags (Hotovec-Ellis et al., 2014). The relation was also briefly noticed in the case of the Pont-Bourquin landslide (Switzerland), but in that case a negative drop in *dv/v* correlated with intense snowfall and snow melting periods (Le Breton, 2019b). A negative drop of *dv/v* was also observed following intense snowfall in eastern Hokkaido (Wang et al., 2017), although the underlying cause remains unclear. This heterogeneity of behavior confirms that the effect of snow on *d/v* should be caused by several processes.

The direct influence of the snow on *dv/v* variations remains poorly understood. A direct elastic loading effect due to the weight of the snowpack is the mechanism most frequently invoked to account for the positive correlation between *dv/v* and snow cover (Hotovec-Ellis et al., 2014; Wang et al., 2017). Several geodetic measurements clearly show deformation of the crust due to loading with snow mass, and subsequent strain changes (Grapenthin et al., 2006; Heki, 2001). These strain changes can be modeled by a poroelastic approach, with a pore pressure wave diffusing in the crust and modulated by the pressure variations due to changes to ice or snow cover at the surface. Snow loading within the crust can also be modeled by a viscous rebound response (Mordret et al., 2016). Although the poroelastic model provides the best fit for the observed lag time of the *dv/v* response, a combination of both poroelastic and viscoelastic effects is expected to explain the negative correlation between *dv/v* and snow cover (Mordret et al., 2016).

Hydrological insulation due to the snow cover can impede water infiltration and limit groundwater recharging (Seiler and Gat, 2007; Wang et al., 2017), and thus can lead to an increase in seismic velocity. However, the mechanisms leading to a negative drop in *dv/v* simultaneously with snowfall are still incompletely known (Wang et al., 2017).

Thermal state is modified by snow, as a result of melting water advection, snow cover insulation, and latent heat release. It is well known and commonly taken into account for landslides and mountainous slope instabilities like rock glaciers (Goodrich, 1982; Staub and Delaloye, 2017). The presence of a thickly packed snow cover induces a thermal insulation buffering heat exchanges between atmosphere and ground, and then modulates the ground thermal state through its timing, duration and thickness. The snow layer could thus change both the water content and the thermal state of surface layers, by slowing soil freezing, while also allowing thawing and moistening of the underlying layers. When snow cover melts, the advection of heat and water within the subsurface decreases the shear modulus, and may also cause *dv/v* to decrease.

The properties of snow on the ground, such as depth, density, water content, structure, and water equivalent, are very heterogeneous in space and time (Bartelt and Lehning, 2002; Fierz et al., 2009). These properties affect the resulting stress, snowmelt water or thermal insulation caused by snow, and therefore influence the *dv/v*. Investigating the effect of snow on *dv/v* should require at least to monitor the snow depth. The other snow properties are more expensive to monitor (Kinar and Pomeroy, 2015; Tedesco, 2015; Pirazzini et al., 2018), and in practice may have to be modeled from meteorological data such as air temperature, solar illumination and wind speed (Bartelt and Lehning, 2002). Instead of measuring snow properties, it

might also be easier measure only its effect on the soil, such as soil superficial stress (due to snow loading), soil temperature (snow insulation) and groundwater levels (snow melting).

It is worth noting that the influence of snow on the apparent *dv/v* may not only be caused by a change of seismic velocity in the bulk material. For example, the presence of snow may create new sources of ambient noise, or might alter the frequency content of noise (by attenuating high frequencies). These effects may distort the partially reconstructed cross-correlation function and lead to apparent *dv/v* that are not related to changes in velocity. These questions should be quantitatively addressed in future studies to reinforce alert systems based on seismological monitoring for mountainous landslides.

5.3.5 Tide

The influence of tide on seismic velocity occurs mostly with cycles of 14, 1 and 0.5 days, as observed for example near a coast and 10 meters under a cliff using underground active transducers measuring variations of V_p (Yamamura et al., 2003). Tidal influence on *dv/v* can be governed by either strain or pore water pressure, depending on the context.

Tide modifies the crustal strain, through earth tide or by water loading caused by ocean tide, causing a relatively small fluctuation of *dv/v*, ranging from 0.02 to 0.6% in the literature. During dilatational (resp. contractional) episodes, respectively, the *dv/v* has been observed to decrease (resp. increase) on volcanoes (Takano et al., 2014, 2019; Mao et al., 2019) similarly to former observation (e.g., Yamamura et al., 2003), and in contrary to increase (resp. decrease) observed on the Piñon Flat Observatory (Hillers et al., 2015c). In any case, the amplitude of strain effect appears negligible compared to other effects on soft soil landslides, particularly shallow ones.

Pore water pressure was suggested to govern the semidiurnal *dv/v* fluctuations, on a sea levee and a sea dike (Planès et al., 2017; Joubert et al., 2018). High marine tide was shown to strongly and clearly decrease *dv/v*, with a 0.5-day periodicity and a non-negligible *dv/v* amplitude of more than 5%. On the sea levee, the *dv/v* correlated perfectly with the pore water pressure measured in situ (Planès et al., 2017). A lag of 40 − 100 minutes occurred between pore pressure and tide level, that was attributed to water diffusion under the levee. The sea dike and see levees were mostly composed of sand and clay, that are similar to soft-soil landslides, and the filtering frequency of the CCFs (5–20 Hz) were in the range of most landslides investigations. Therefore, on coastal landslides (e.g., Francioni et al., 2018), marine tide might play a significant role on *dv/v* observed, due to changes of groundwater levels at its base (but is already negligible a few km from the coast). Lastly, atmospheric tide, that varies by ~ 1% within 12h, can activate a periodic semidiurnal displacement on a few landslides (Schulz et al., 2009). This displacement is supposedly caused by pressure imbalance induced by the

slowness of the diffusion of the tidal atmospheric pressure changes within the pores. Such effect might potentially influence the *dv/v* on the landslides where it occurs, but with amplitudes that we expect negligible on most landslides, compared to other environmental influences.

6 Landslide triggers

To effectively monitor a landslide, precursor signals before a potential failure must be discriminated from non-precursor environmental influences. Two precursor phenomena have been studied so far with ambient noise correlations: the liquefaction of clayey layers and the combined effect of earthquakes together with precipitations.

6.1 Rainfall-induced fluidization

Fluidization of landslide material was observed to turn clay-rich landslides to mudflows or debris flows (Van Asch and Malet, 2009) following heavy rainfalls (Iverson et al., 1997). The mechanisms of fluidization of clayey soils can be explained by viscoplastic laws (Huang and García, 1998), with the soil behaving as a soft solid when the static shear stress applied is below the yield stressτ_c, and as a viscous fluid above that limit. Fluidization can also be triggered by an increase in the water content, above the so-called Atterberg liquid limit with zero stress. These two indicators (τ_c and water content) are related. Indeed, the critical stress τ_c decreases when the water content of the soil increases (Coussot, 1995). This relationship has been confirmed on a Trièves landslide soil (Fig. 21) and was consistent across six landslide soils (Carrière et al., 2018b). In short, landslide fluidization can be triggered by an increase in either the shear stress or the water content.

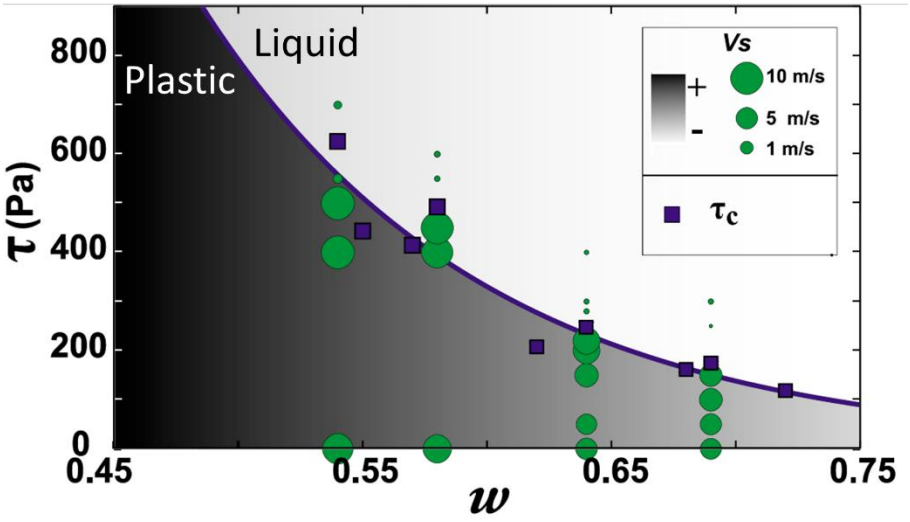

Fig. 20: Critical stress as a function of the gravimetric water content *w* on soil samples from Trièves clayey soil. The critical stress was either measured (blue squares) or fitted with an exponential law (Coussot, 1995). The shear-wave velocity Vs was measured for specific water content and stress values, and its value is represented by the size of the green circles. Vs is represented qualitatively in the background by the dark shadow, representing higher Vs values. From (Mainsant et al., 2012a).

Shear-wave velocity should decrease during fluidization, because of the reduced rigidity, if the material density remains constant (see eq. (1)). Indeed, on fluidization-prone landslides, reduced shear-wave velocity has been observed in faster-moving zones (Jongmans et al., 2009; Renalier et al., 2010b) before dramatic accelerations (Mainsant et al., 2012b), and immediately after such accelerations (Bertello et al., 2018; Berti et al., 2019). To further analyze these observations, laboratory tests were carried out on soil samples from seven landslides known to have undergone fluidization in the past. The laboratory experiments showed shear-wave velocity to decrease by up to 8% when the sample shifted from a plastic to a viscous behavior (Carrière et al., 2018b, 2018a; Mainsant et al., 2015, 2012a). Therefore, the fluidization of clayey materials leads to a decrease in the *dv/v* that exceeds yearly environmental variations (1–5% observed on landslides, see Fig. 14). Consequently, ambient noise correlation could be used to monitor fluidization-prone landslides.

The precursory nature of the velocity drop observed before a dramatic acceleration was suggested by Mainsant et al. (2012b). However, two questions remained: Is the precursor signal reproducible under controlled conditions? Is the drop in velocity precursory to or concomitant with the displacement? (The time resolution for the displacement measured during the failure of Pont-Bourquin in 2010 was not high enough to answer this question). Mainsant et al. (2015), followed by Carrière et al. (2018a), performed laboratory experiments to monitor the velocity of shear waves over time in soil samples taken from various landslides. In their tests, they progressively increased the shear stress applied to samples with different water contents. They observed that a decrease in Vs, a distinctive feature of the solid-fluid transition of the soil, was consistently observed before any measurable displacements (e.g., Fig. 19).

These observations confirm that decreases in shear-wave velocity are a precursor to fluidization of the soil. However, in these experiments, fluidization resulted from increasing stress, and not water content as it would occur in the field. The precursory nature of the velocity drop therefore needs to be further confirmed, for example with a rain-controlled flume simulation (e.g., Wang and Sassa, 2003), and compared to standard predictive methods such as the inverse of the displacement rate (Intrieri et al., 2019).

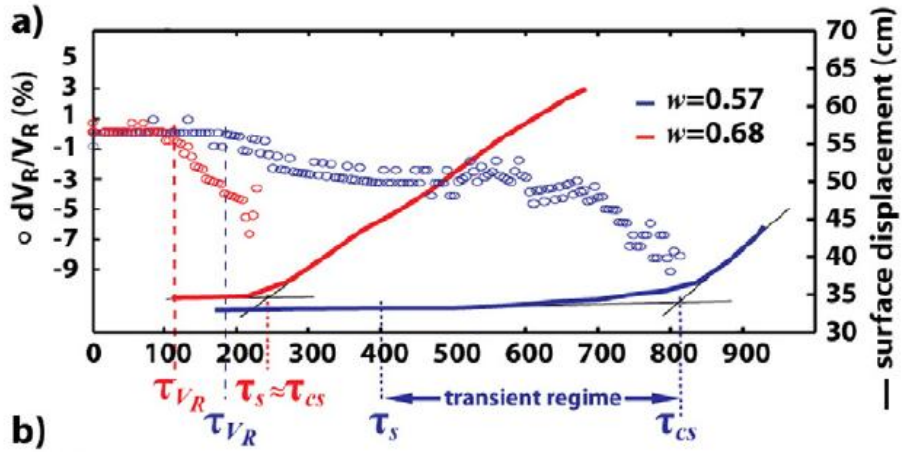

Fig. 21: Influence of the shear stress τ applied on the apparent Rayleigh velocity variation dV_R/V_R (dots) and surface displacement (continuous lines). Flume experiments were performed in the laboratory, with two different water contents *w*. The results confirm the joint influence of shear stress and water content on the liquid-plastic threshold, and that the V_R starts to decrease at a stress τ_{V_R} before surface displacement (strain) is triggered at τ_s. From (Mainsant et al., 2015).

Reduced shear-wave velocity has been observed multiple times on the Montevecchio earth flow (Bertello et al., 2018) and on six other landslides in the same region (Berti et al., 2019) following fluidization of the soil, using the active MASW and passive ReMI methods (Park et al., 1999; Louie, 2001). These observations emphasize the strong impact the fluidization of the landslide has on shear-wave velocity, with a considerable drop in Rayleigh wave velocity (−30% to −40%). This value is much higher than the –7% observed at Pont-Bourquin: on this landslide, the material affected was limited to a thin layer at depth, whereas in Montevecchio the whole structure was affected. Interestingly, these studies also highlight the usefulness of Vs for slope consolidation once fluidization has occurred. Indeed, after the rapid decrease in shear-wave velocities due to fluidization of the soil, a progressive increase (recovery) of the Rayleigh waves was observed in the landslide's bulk as the earth flows slowed down. The authors linked this phenomenon to the consolidation of the slope material (Bertello et al., 2018; Berti et al., 2019) (see Fig. 20). In short, recordings of the shear-wave velocity could thus be used to monitor the progressive consolidation of the slope material after a rapid flow event.

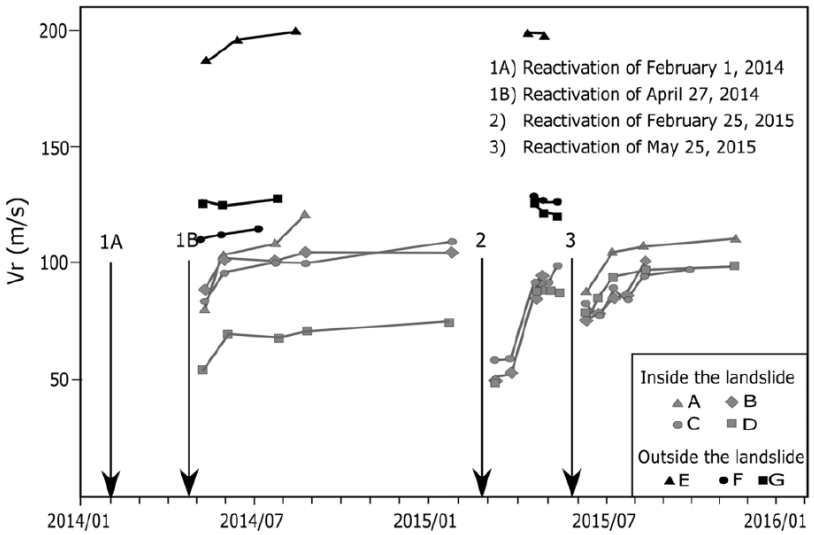

Fig. 22: Rayleigh wave velocity measured at a depth of 2 m using the MAWS and the ReMi techniques during repeated surveys of the Montevecchio earth flow at several locations. Arrows show the start of the main reactivation events. The velocity inside the landslide appears to drop after reactivations, with a recovery period of several weeks before returning to its original value. From (Bertello et al., 2018).

6.2 Earthquakes

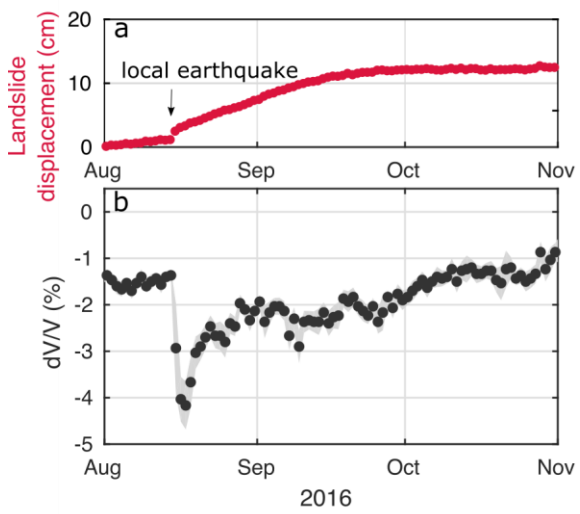

Fig. 23: (a) Landslide displacement generated by an earthquake in the vicinity of a landslide (~10 km) and (b) decrease of the apparent seismic velocity recorded at the landslide following the event. Redrawn from (Bontemps et al., 2020)

Strong decreases in seismic wave velocity have consistently been observed after major earthquakes (Brenguier et al., 2008a; Obermann et al., 2014; Richter et al., 2014; Gassenmeier et al., 2015a; Viens et al., 2018). The amplitude of the variations observed for a given event can vary from 0.1% (Brenguier et al., 2014) to more than 10% (Nakahara, 2015; Nakata and Snieder, 2011), depending on the investigation depth and the distance between the seismometer and the source of the earthquake (Viens et al., 2018). Following the co-seismic drop, the ground consistently undergoes a recovery phase, characterized by an increase in the

dv/v, which often returns to its pre-earthquake value (Richter et al., 2014; Gassenmeier et al., 2016). This recovery phase has also been observed at laboratory scale (TenCate, 2011), and is referred to as "slow dynamic" recovery. Both in the laboratory and after large earthquakes, the recovery phase was shown to follow a pseudo-logarithmic shape over time (TenCate, 2011; Richter et al., 2014; Gassenmeier et al., 2015a; Snieder et al., 2017; Viens et al., 2018). Bontemps et al. (2020) revealed that even moderate earthquakes (Mw ≤ 5.5) can affect the surface wave velocity on a landslide. Thus, on the slow-moving Maca landslide (< 1 m/year in 2016–2018) in Peru, a local earthquake of magnitude 5.5 located 10 km away abruptly reduced the *dv/v* by 3% (Fig. 23). This seismic event also generated a co-seismic slip of 1 cm, followed by an 11-cm displacement one month after the earthquake. A recovery phase was then observed, which fitted the model proposed by Richter et al. (2014).

Strong ground motion caused by earthquakes generates a nonlinear response within the soil, which decreases its elastic modulus and diminishes the seismic velocity (Beresnev and Wen, 1996). In extreme cases, plastic deformation can occur, leading to soil liquefaction (Keefer, 1984). The drop in soil rigidity following strong shaking may be due to the generation of macro- and micro-cracks in the medium (Ostrovsky and Johnson, 2001; Rojstaczer and Wolf, 1992) or to the rearrangement of the grains due to weak inter-grain contacts (Ostrovsky and Johnson, 2001; Tournat et al., 2004). The slow dynamic effect corresponds to healing of the soil by the progressive closing of cracks, and the rearrangement and cementation of grains (Gassenmeier et al., 2016; Viens et al., 2018) progressively returning to their initial state.

Several studies have attempted to determine the *dv/v* trend during and after earthquakes to better understand the parameters controlling damage to the ground over time. Richter et al. (2014) fitted a logarithmic curve to the *dv/v* drop observed on the day of a major earthquake. Once long (seasonal or tectonic) trends had been removed from the signal, they found a linear relationship between the transient velocity changes and the peak ground acceleration caused by smaller events at a given station (Richter et al., 2014). Gassenmeier et al. (2016) inferred that small vibrations as well as large earthquakes can decrease the rigidity of the material. Therefore, they integrated the envelope of the ground acceleration over one day instead of the peak ground acceleration alone, to model the expected drop in *dv/v* during an earthquake. They subsequently modeled the recovery using an exponential curve rather than a logarithmic curve (Snieder et al., 2017). This model has the advantage of converging toward a finite limit at long times, and thus better represents the real state of the soil once completely healed (Gassenmeier et al., 2016). Nevertheless, the ambient noise correlation technique has only relatively recently been adopted to study the impact of earthquakes on landslides, and many questions remain. Can we also find a relation between the *dv/v* drop and the peak ground ac-

celeration measured on the landslide like that described by Richter et al. (2014)? Can the presence of water in the landslide also affect the *dv/v* drop generated by the shaking, as observed by Brenguier et al. (2014) on volcanoes? Does the recovery process always follow a logarithmic shape with time? Can other processes specific to landslides, such as displacement or changes to the preferential flow of water after an earthquake, affect how the material recovers?

In summary, earthquakes affect the *dv/v* measured on landslides. The amplitude of the drop in *dv/v* depends on the frequency band studied (i.e., the investigation depth) and the distance between the earthquake and the landslide. An extensive drop in *dv/v* can be expected for local moderate earthquakes or remote large earthquakes. The sudden 3% velocity drop that followed the magnitude 5.5 earthquake 10 km from Maca was clearly identifiable within the slow seasonal fluctuations (*dv/v* ≈ 2%). This type of velocity drop could give an indication of the potential risk of landslides being triggered during and for several days after an earthquake.

6.3 Stability indicators before and after an event

Slow-moving landslides may either accelerate or stabilize under the influence of external factors such as rainfall, earthquakes or human interventions (Lacroix et al., 2012). Extending the proposal of Bontemps et al. (2020), we suggest that the following four states of a landslide can be related to a *dv/v* value (Fig. 24): stable, moving, critical, and failure. In the stable state, the landslide is not moving. On landslides that activate after a precipitation threshold, such as Maca (Bontemps et al., 2018; Zerathe et al., 2016), the landslide can remain stable despite minor earthquakes or rainfall.

In the creeping state, the displacement rate is linear with respect to the rainfall rate convolved with a fixed impulse response (Helmstetter and Garambois, 2010; Belle et al., 2014; Bernardie et al., 2015; Le Breton, 2019a). This state also corresponds to the classical primary and secondary creep of landslides (Intrieri et al., 2019). The transition from stable to creeping state, and its reverse, corresponded to the *dv/v* crossing a threshold on the Maca deep-seated landslide (Bontemps et al., 2020). In the latter study, the transition from stable to moving was triggered both by rainfall and seismic events. Bontemps et al. (2020) observed that, over 2.5 years in 2016–2018, the Maca landslide moved only when the *dv/v* dropped below a threshold (-1.2% at 3 − 8 Hz), and stopped moving when it once again exceeded this threshold as it recovered.

In the critical state, the amplitude of the impulse response increases, leading to a higher displacement rate after the same rainfall (Le Breton, 2019a); this increased displacement rate can be a precursory signal before failure (Bernardie et al., 2015). The critical state corresponds to the tertiary creep phase occurring before a failure (Intrieri et al., 2019). The creeping-to-

critical transition, and its reverse, is suggested on the Pont-Bourquin landslide, where a decrease in *dv/v* of 1 − 2% at 10 − 14 Hz (no threshold identified) correlates with a doubling of the landslide displacement following the same rainfall input (Le Breton, 2019a).

Finally, failure corresponds to extremely rapid and nonlinear landslide displacements. The critical-to-failure transition was observed on the Pont-Bourquin landslide, when the *dv/v* decreased below −5% at 10 − 12 Hz before the failure (Mainsant et al., 2012b). The reverse, the failure-to-metastable transition, corresponds to the recovery observed on the Montevecchio earthflow (Bertello et al., 2018) where the *dv/v* slowly increased from about −30% back to 0%

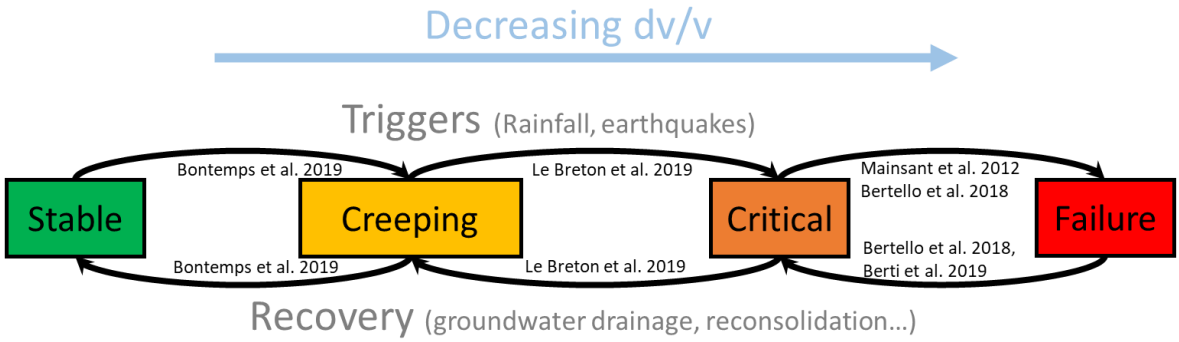

Fig. 24: Four states proposed for a creeping landslide, with transitions related to the dv/v.

In addition to precursory signals, the *dv/v* indicator can be used to observe how a landslide recovers. As previously mentioned, a slow recovery of the shear-wave velocity has been reported both after an earthquake shaking (Bontemps et al., 2020), or after fluidization triggered by rainfall (Bertello et al., 2018; Berti et al., 2019). During recovery, the apparent velocity progressively (within weeks or months) returned to its original value, while the landslide transitioned from creeping to stable state. Recovery may take years to complete, as observed on non-landslide sites (Gassenmeier et al., 2016). Monitoring recovery should help to determine when an unstable slope has become stable once again, after a critical event such as a failure, a period of heavy rainfall, stabilization work (e.g., drainage), an explosion, or an earthquake. That could also be helpful for designing risk-management strategies, for example to support a decision of reopening a road after a landslide acceleration.

Nevertheless, in current practice, no geophysical method provides certain precursors for use in an early-warning system. Therefore, multiple geophysical indicators (microseismicity, resonance frequency, *dv/v*, *CC*) should be monitored simultaneously to increase the robustness of warnings. In all cases, any alert system would have to include surface observations (Intrieri et al., 2019), such as extensometry, GPS, or recently RFID (Angeli et al., 2000; Gili et al., 2000;

Le Breton et al., 2019) to allow comparison of bulk mechanical variations to surface deformations.

Conclusion

The present review covers studies performed on nine long-term investigations of landslides using ambient noise correlation, and focuses on early-warning applications: using robust processing, improving the time resolution below a day, and understanding environmental fluctuations. Depending on the site studied, it might be necessary to check for the stability of the noise source (in space, azimuth, and frequency content), for changes to resonance frequencies or the scattering structure of the propagating medium, for accurate synchronization, and for the stability of inter-sensor distance. The main processing parameters to be adapted to each landslide are the time window and the filtering frequency of the correlation functions over which the velocity is computed.

Apparent velocity may fluctuate due to changes in the noise field, to reversible environmental influences, or to triggering factors. For the noise field, we recommend checking for source fluctuations, source anisotropy, and resonance frequencies, before interpreting variations in apparent velocity, to avoid any spurious influences. If problems are identified, we suggest avoiding the resonance frequency, distinguishing between seismic events and sources, and using a network of sensors as pseudo-sources. Reversible environmental influences can be monitored based on the amplitude of seasonal fluctuations, which happens to follow a linear trend with the filtering frequency (from a few hundredths of % to a few %).

Several environmental factors can cause a reversible fluctuation of the seismic velocity, either seasonal or daily. Understanding their influence will allow to better distinguish these fluctuations from precursory signal before landslide failures. The influence of groundwater levels and soil freezing/thawing on these fluctuations was consistent across studies, but the effects of temperature, snow and tide remain to be investigated. The two major landslide triggers—fluidization due to rainfall and earthquakes—were both observed to decrease the seismic velocity, during which landslides were observed to accelerate. After an acceleration event, the seismic velocity slowly recovered back to its initial value, which is explained by the progressive reconsolidation of the landslide material.

Future developments could focus on confirming the relation between dv/v and landslide triggers (earthquakes and soil fluidization) on additional sites, correcting for environmental variations and studying their variations at a sub-daily time resolution. The effect of snow deposition and melting should also be studied in detail, as the impact of these major triggering factors on the apparent velocity remains unclear. In the cases reported, nevertheless, the decreases in velocity observed prior to or during failure were larger than other effects.

Acknowledgments

We acknowledge funding and support from the French National Agency for research (ANR) through the LABCOM Geo3iLab project (ANR- 17- LCV2-0007-01), from the Labex OSUG@2020, and from the companies Géolithe and Géolithe Innov. We thank C. Voisin, D. Jongmans, G. Bièvre, and P. Lacroix for fruitful discussions, B. Vial and M. Langlais for engineering support when updating the Pont-Bourquin data, and M. Gallagher for proofreading.

References

Abraham, O., Piwakowski, B., Villain, G., Durand, O., 2012. Non-contact, automated surface wave measurements for the mechanical characterisation of concrete. Construction and Building Materials, Non Destructive Techniques for Assessment of Concrete 37, 904–915. https://doi.org/10.1016/j.conbuildmat.2012.03.015

Alimohammadlou, Y., Najafi, A., Yalcin, A., 2013. Landslide process and impacts: A proposed classification method. CATENA 104, 219–232. https://doi.org/10.1016/j.catena.2012.11.013

Amitrano, D., Gaffet, S., Malet, J.-P., Maquaire, O., 2007. Understanding mudslides through micro-seismic monitoring: the Super-Sauze (South-East French Alps) case study. Bulletin de la Société Géologique de France 178, 149–157. https://doi.org/10.2113/gssgfbull.178.2.149

Amitrano, D., Grasso, J.R., Senfaute, G., 2005. Seismic precursory patterns before a cliff collapse and critical point phenomena. Geophysical Research Letters 32. https://doi.org/10.1029/2004GL022270

Anderson, O.L., Schreiber, E., Liebermann, R.C., Soga, N., 1968. Some elastic constant data on minerals relevant to geophysics. Reviews of Geophysics 6, 491–524. https://doi.org/10.1029/RG006i004p00491

Angeli, M.-G., Pasuto, A., Silvano, S., 2000. A critical review of landslide monitoring experiences. Engineering Geology 55, 133–147. https://doi.org/10.1016/S0013-7952(99)00122-2

Bartelt, P., Lehning, M., 2002. A physical SNOWPACK model for the Swiss avalanche warning: Part I: numerical model. Cold Regions Science and Technology 35, 123–145. https://doi.org/10.1016/S0165-232X(02)00074-5

Belle, P., Aunay, B., Bernardie, S., Grandjean, G., Ladouche, B., Mazué, R., Join, J.-L., 2014. The application of an innovative inverse model for understanding and predicting landslide movements (Salazie cirque landslides, Reunion Island). Landslides 11, 343–355. https://doi.org/10.1007/s10346-013-0393-5

Bensen, G.D., Ritzwoller, M.H., Barmin, M.P., Levshin, A.L., Lin, F., Moschetti, M.P., Shapiro, N.M., Yang, Y., 2007. Processing seismic ambient noise data to obtain reliable broad-band surface wave dispersion measurements. Geophys J Int 169, 1239–1260. https://doi.org/10.1111/j.1365-246X.2007.03374.x

Beresnev, I.A., Wen, K.-L., 1996. Nonlinear soil response—A reality? Bulletin of the Seismological Society of America 86, 1964–1978.

Berger, J., 1975. A note on thermoelastic strains and tilts. Journal of Geophysical Research (1896-1977) 80, 274–277. https://doi.org/10.1029/JB080i002p00274

Bernardie, S., Desramaut, N., Malet, J.-P., Gourlay, M., Grandjean, G., 2015. Prediction of changes in landslide rates induced by rainfall. Landslides 12, 481–494. https://doi.org/10.1007/s10346-014-0495-8

Bertello, L., Berti, M., Castellaro, S., Squarzoni, G., 2018. Dynamics of an Active Earthflow Inferred From Surface Wave Monitoring. Journal of Geophysical Research: Earth Surface 123, 1811–1834. https://doi.org/10.1029/2017JF004233

Berti, M., Bertello, L., Squarzoni, G., 2019. Surface-wave velocity measurements of shear stiffness of moving earthflows. Landslides 16, 469–484. https://doi.org/10.1007/s10346-018-1102-1

Bièvre, G., Franz, M., Larose, E., Carrière, S., Jongmans, D., Jaboyedoff, M., 2018. Influence of environmental parameters on the seismic velocity changes in a clayey mudflow (Pont-Bourquin Landslide, Switzerland). Engineering Geology 245, 248–257. https://doi.org/10.1016/j.enggeo.2018.08.013

Biot, M.A., 1962. Mechanics of deformation and acoustic propagation in porous media. Journal of applied physics 33, 1482–1498.

Bonnefoy-Claudet, S., Cotton, F., Bard, P.-Y., 2006. The nature of noise wavefield and its applications for site effects studies. Earth-Science Reviews 79, 205–227. https://doi.org/10.1016/j.earscirev.2006.07.004

Bontemps, N., Lacroix, P., Doin, M.-P., 2018. Inversion of deformation fields time-series from optical images, and application to the long term kinematics of slow-moving landslides in

Peru. Remote Sensing of Environment 210, 144–158. https://doi.org/10.1016/j.rse.2018.02.023

Bontemps, N., Lacroix, P., Larose, E., Jara, J., Taipe, E., 2020. Rain and small earthquakes maintain a slow-moving landslide in a persistent critical state. Nat Commun 11, 1–10. https://doi.org/10.1038/s41467-020-14445-3

Bontemps, N., Lacroix, P., Larose, E., Jara, J., Taipe, E., in preparation. Rain and small earthquakes can maintain a slow moving landslide in critical state.

Bottelin, P., Baillet, L., Larose, E., Jongmans, D., Hantz, D., Brenguier, O., Cadet, H., Helmstetter, A., 2017. Monitoring rock reinforcement works with ambient vibrations: La Bourne case study (Vercors, France). Engineering Geology 226, 136–145. https://doi.org/10.1016/j.enggeo.2017.06.002

Bottelin, P., Jongmans, D., Baillet, L., Lebourg, T., Hantz, D., Levy, C., Le Roux, O., Cadet, H., Lorier, L., Rouiller, J.-D., Turpin, J., Darras, L., 2013a. Spectral Analysis of Prone-to-fall Rock Compartments using Ambient Vibrations. Journal of Environmental & Engineering Geophysics 18, 205–217. https://doi.org/10.2113/JEEG18.4.205

Bottelin, P., Lévy, C., Baillet, L., Jongmans, D., Guéguen, P., 2013b. Modal and thermal analysis of Les Arches unstable rock column (Vercors massif, French Alps). Geophys J Int 194, 849–858. https://doi.org/10.1093/gji/ggt046

Brenguier, F., Campillo, M., Hadziioannou, C., Shapiro, N.M., Nadeau, R.M., Larose, E., 2008a. Postseismic Relaxation Along the San Andreas Fault at Parkfield from Continuous Seismological Observations. Science 321, 1478–1481. https://doi.org/10.1126/science.1160943

Brenguier, F., Campillo, M., Takeda, T., Aoki, Y., Shapiro, N.M., Briand, X., Emoto, K., Miyake, H., 2014. Mapping pressurized volcanic fluids from induced crustal seismic velocity drops. Science 345, 80–82. https://doi.org/10.1126/science.1254073

Brenguier, F., Clarke, D., Aoki, Y., Shapiro, N.M., Campillo, M., Ferrazzini, V., 2011. Monitoring volcanoes using seismic noise correlations. Comptes Rendus Geoscience 343, 633–638. https://doi.org/10.1016/j.crte.2010.12.010

Brenguier, F., Rivet, D., Obermann, A., Nakata, N., Boué, P., Lecocq, T., Campillo, M., Shapiro, N., 2016. 4-D noise-based seismology at volcanoes: Ongoing efforts and perspectives. Journal of Volcanology and Geothermal Research 321, 182–195. https://doi.org/10.1016/j.jvolgeores.2016.04.036

Brenguier, F., Shapiro, N.M., Campillo, M., Ferrazzini, V., Duputel, Z., Coutant, O., Nercessian, A., 2008b. Towards forecasting volcanic eruptions using seismic noise. Nature Geoscience 1, 126–130. https://doi.org/10.1038/ngeo104

Brönnimann, C.S., 2011. Effect of Groundwater on Landslide Triggering (Ph.D. Thesis). École Polytechnique Fédérale de Lausanne, Switzerland.

Burjánek, J., Gassner‐Stamm, G., Poggi, V., Moore, J.R., Fäh, D., 2010. Ambient vibration analysis of an unstable mountain slope. Geophysical Journal International 180, 820‐828. https://doi.org/10.1111/j.1365-246X.2009.04451.x

Burjánek, J., Moore, J.R., Yugsi Molina, F.X., Fäh, D., 2012. Instrumental evidence of normal mode rock slope vibration. Geophys J Int 188, 559–569. https://doi.org/10.1111/j.1365-246X.2011.05272.x

Campillo, M., Paul, A., 2003. Long-Range Correlations in the Diffuse Seismic Coda. Science 299, 547–549. https://doi.org/10.1126/science.1078551

Carrière, S.R., Bièvre, G., Jongmans, D., Chambon, G., Bellot, H., Lebourg, T., 2018a. Measurement of geophysical parameters on clay samples at the solid–fluid transition. Near Surface Geophysics 16, 1–15. https://doi.org/10.3997/1873-0604.2017039

Carrière, S.R., Jongmans, D., Chambon, G., Bièvre, G., Lanson, B., Bertello, L., Berti, M., Jaboyedoff, M., Malet, J.-P., Chambers, J.E., 2018b. Rheological properties of clayey soils originating from flow-like landslides. Landslides 15, 1615–1630. https://doi.org/10.1007/s10346-018-0972-6

Clements, T., Denolle, M.A., 2018. Tracking Groundwater Levels Using the Ambient Seismic Field. Geophysical Research Letters 45, 6459–6465. https://doi.org/10.1029/2018GL077706

Colombero, C., Baillet, L., Comina, C., Jongmans, D., Larose, E., Valentin, J., Vinciguerra, S., 2018. Integration of ambient seismic noise monitoring, displacement and meteorological measurements to infer the temperature-controlled long-term evolution of a complex prone-to-fall cliff. Geophys J Int 213, 1876–1897. https://doi.org/10.1093/gji/ggy090

Coussot, P., 1995. Structural Similarity and Transition from Newtonian to Non-Newtonian Behavior for Clay-Water Suspensions. Phys. Rev. Lett. 74, 3971–3974. https://doi.org/10.1103/PhysRevLett.74.3971

Dai, F.C., Lee, C.F., Ngai, Y.Y., 2002. Landslide risk assessment and management: an overview. Engineering Geology 64, 65–87. https://doi.org/10.1016/S0013-7952(01)00093-X

Danneels, G., Bourdeau, C., Torgoev, I., Havenith, H.-B., 2008. Geophysical investigation and dynamic modelling of unstable slopes: case-study of Kainama (Kyrgyzstan). Geophys J Int 175, 17–34. https://doi.org/10.1111/j.1365-246X.2008.03873.x

Daskalakis, E., Evangelidis, C.P., Garnier, J., Melis, N.S., Papanicolaou, G., Tsogka, C., 2016. Robust seismic velocity change estimation using ambient noise recordings. Geophysical Journal International 205, 1926–1936.

Del Gaudio, V., Muscillo, S., Wasowski, J., 2014. What we can learn about slope response to earthquakes from ambient noise analysis: An overview. Engineering Geology, Special Issue on The Long-Term Geologic Hazards in Areas Struck by Large-Magnitude Earthquakes 182, 182–200. https://doi.org/10.1016/j.enggeo.2014.05.010

Delaney, E., Ermert, L., Sager, K., Kritski, A., Bussat, S., Fichtner, A., 2017. Passive seismic monitoring with nonstationary noise sources. GEOPHYSICS 82, KS57–KS70. https://doi.org/10.1190/geo2016-0330.1

Dong, Y., Lu, N., 2016. Dependencies of Shear Wave Velocity and Shear Modulus of Soil on Saturation. Journal of Engineering Mechanics 142, 04016083. https://doi.org/10.1061/(ASCE)EM.1943-7889.0001147

Draganov, D., Campman, X., Thorbecke, J., Verdel, A., Wapenaar, K., 2013. Seismic exploration-scale velocities and structure from ambient seismic noise (>1 Hz). Journal of Geophysical Research: Solid Earth 118, 4345–4360. https://doi.org/10.1002/jgrb.50339

Draganov, D., Wapenaar, K., Mulder, W., Singer, J., Verdel, A., 2007. Retrieval of reflections from seismic background-noise measurements. Geophysical Research Letters 34. https://doi.org/10.1029/2006GL028735

Duputel, Z., Ferrazzini, V., Brenguier, F., Shapiro, N., Campillo, M., Nercessian, A., 2009. Real time monitoring of relative velocity changes using ambient seismic noise at the Piton de la Fournaise volcano (La Réunion) from January 2006 to June 2007. Journal of Volcanology and Geothermal Research, Recent advances on the geodynamics of Piton de la Fournaise volcano 184, 164–173. https://doi.org/10.1016/j.jvolgeores.2008.11.024

Fichtner, A., Stehly, L., Ermert, L., Boehm, C., 2017. Generalized interferometry – I: theory for interstation correlations. Geophys J Int 208, 603–638. https://doi.org/10.1093/gji/ggw420

Fierz, C., Amstrong, R.L., Durand, Y., Etchevers, P., Greene, E., McClung, D.M., Nishimura, K., Satyawali, P.K., Sokratov, S.A., 2009. The International Classification for Seasonal Snow on the Ground (No. IHP-VII Technical Documents in Hydrology N°83, IACS Contribution N°1). UNESCO-IHP, Paris.

Fiolleau, S., Jongmans, D., Bièvre, G., Chambon, G., Baillet, L., Vial, B., 2020. Seismic characterization of a clay-block rupture in Harmalière landslide, French Western Alps. Geophysical Journal International 221, 1777–1788. https://doi.org/10.1093/gji/ggaa050

Flores Orozco, A., Bücker, M., Steiner, M., Malet, J.-P., 2018. Complex-conductivity imaging for the understanding of landslide architecture. Engineering Geology 243, 241–252. https://doi.org/10.1016/j.enggeo.2018.07.009

Francioni, M., Coggan, J., Eyre, M., Stead, D., 2018. A combined field/remote sensing approach for characterizing landslide risk in coastal areas. International Journal of Applied Earth Observation and Geoinformation 67, 79–95. https://doi.org/10.1016/j.jag.2017.12.016

Froment, B., Campillo, M., Roux, P., Gouédard, P., Verdel, A., Weaver, R., 2010. Estimation of the effect of nonisotropically distributed energy on the apparent arrival time in correlations. GEOPHYSICS 75, SA85–SA93. https://doi.org/10.1190/1.3483102

Froude, M.J., Petley, D.N., 2018. Global fatal landslide occurrence from 2004 to 2016. Natural Hazards and Earth System Sciences 18, 2161–2181. https://doi.org/10.5194/nhess-18-2161-2018

Gaffet, S., Guglielmi, Y., Cappa, F., Pambrun, C., Monfret, T., Amitrano, D., 2010. Use of the simultaneous seismic, GPS and meteorological monitoring for the characterization of a large unstable mountain slope in the southern French Alps. Geophys J Int 182, 1395–1410. https://doi.org/10.1111/j.1365-246X.2010.04683.x

Gallistl, J., Weigand, M., Stumvoll, M., Ottowitz, D., Glade, T., Orozco, A.F., 2018. Delineation of subsurface variability in clay-rich landslides through spectral induced polarization imaging and electromagnetic methods. Engineering Geology 245, 292–308. https://doi.org/10.1016/j.enggeo.2018.09.001

Gariano, S.L., Guzzetti, F., 2016. Landslides in a changing climate. Earth-Science Reviews 162, 227–252. https://doi.org/10.1016/j.earscirev.2016.08.011

Garnier, V., Piwakowski, B., Abraham, O., Villain, G., Payan, C., Chaix, J.F., 2013. Acoustic techniques for concrete evaluation: Improvements, comparisons and consistency. Construction and Building Materials 43, 598–613. https://doi.org/10.1016/j.conbuildmat.2013.01.035

Gassenmeier, M., Sens-Schönfelder, C., Delatre, M., Korn, M., 2015a. Monitoring of environmental influences on seismic velocity at the geological storage site for CO2 in Ketzin (Germany) with ambient seismic noise. Geophys J Int 200, 524–533. https://doi.org/10.1093/gji/ggu413

Gassenmeier, M., Sens-Schönfelder, C., Delatre, M., Korn, M., 2015b. Monitoring of environmental influences on seismic velocity at the geological storage site for CO2 in Ketzin (Germany) with ambient seismic noise. Geophys J Int 200, 524–533. https://doi.org/10.1093/gji/ggu413

Gassenmeier, M., Sens-Schönfelder, C., Eulenfeld, T., Bartsch, M., Victor, P., Tilmann, F., Korn, M., 2016. Field observations of seismic velocity changes caused by shaking-induced damage and healing due to mesoscopic nonlinearity. Geophys J Int 204, 1490–1502. https://doi.org/10.1093/gji/ggv529

Gili, J.A., Corominas, J., Rius, J., 2000. Using Global Positioning System techniques in landslide monitoring. Engineering Geology 55, 167–192. https://doi.org/10.1016/S0013-7952(99)00127-1

Gimbert, F., Tsai, V.C., Amundson, J.M., Bartholomaus, T.C., Walter, J.I., 2016. Subseasonal changes observed in subglacial channel pressure, size, and sediment transport. Geophysical Research Letters 43, 3786–3794.

Goodrich, L.E., 1982. The influence of snow cover on the ground thermal regime. Can. Geotech. J. 19, 421–432. https://doi.org/10.1139/t82-047

Grapenthin, R., Sigmundsson, F., Geirsson, H., Árnadóttir, T., Pinel, V., 2006. Icelandic rhythmics: Annual modulation of land elevation and plate spreading by snow load. Geophysical Research Letters 33. https://doi.org/10.1029/2006GL028081

Grêt, A., Snieder, R., Scales, J., 2006a. Time-lapse monitoring of rock properties with coda wave interferometry. Journal of Geophysical Research: Solid Earth 111. https://doi.org/10.1029/2004JB003354

Grêt, A., Snieder, R., Scales, J., 2006b. Time-lapse monitoring of rock properties with coda wave interferometry: TIME-LAPSE MONITORING OF ROCK PROPERTIES. J. Geophys. Res. 111, n/a-n/a. https://doi.org/10.1029/2004JB003354

Guillemot, A., Helmstetter, A., Larose, É., Baillet, L., Garambois, S., Mayoraz, R., Delaloye, R., 2020. Seismic monitoring in the Gugla rock glacier (Switzerland): ambient noise correlation, microseismicity and modelling. Geophys J Int 221, 1719–1735. https://doi.org/10.1093/gji/ggaa097

Hadziioannou, C., 2011. Ondes sismiques en milieu complexe : mesure des variations temporelles des vitesses (phdthesis). Université de Grenoble.

Hadziioannou, C., Larose, E., Baig, A., Roux, P., Campillo, M., 2011. Improving temporal resolution in ambient noise monitoring of seismic wave speed. Journal of Geophysical Research: Solid Earth 116. https://doi.org/10.1029/2011JB008200

Hadziioannou, C., Larose, E., Coutant, O., Roux, P., Campillo, M., 2009. Stability of monitoring weak changes in multiply scattering media with ambient noise correlation: Laboratory experiments. The Journal of the Acoustical Society of America 125, 3688–3695.

Harba, P., Pilecki, Z., 2017. Assessment of time–spatial changes of shear wave velocities of flysch formation prone to mass movements by seismic interferometry with the use of ambient noise. Landslides 14, 1225–1233. https://doi.org/10.1007/s10346-016-0779-2

Harba, P., Pilecki, Z., Krawiec, K., 2019. Comparison of MASW and seismic interferometry with use of ambient noise for estimation of S-wave velocity field in landslide subsurface. Acta Geophys. https://doi.org/10.1007/s11600-019-00344-9

Häusler, M., Michel, C., Burjánek, J., Fäh, D., 2019. Fracture Network Imaging on Rock Slope Instabilities Using Resonance Mode Analysis. Geophysical Research Letters 46, 6497–6506. https://doi.org/10.1029/2019GL083201

Heki, K., 2001. Seasonal Modulation of Interseismic Strain Buildup in Northeastern Japan Driven by Snow Loads. Science 293, 89–92. https://doi.org/10.1126/science.1061056

Helmstetter, A., Garambois, S., 2010. Seismic monitoring of Séchilienne rockslide (French Alps): Analysis of seismic signals and their correlation with rainfalls. Journal of Geophysical Research: Earth Surface 115. https://doi.org/10.1029/2009JF001532

Hennino, R., Trégourès, N., Shapiro, N.M., Margerin, L., Campillo, M., Tiggelen, B.A. van, Weaver, R.L., 2001. Observation of equipartition of seismic waves. Physical review letters 86, 3447–3450. https://doi.org/10.1103/PhysRevLett.86.3447

Hillers, G., Ben-Zion, Y., Campillo, M., Zigone, D., 2015a. Seasonal variations of seismic velocities in the San Jacinto fault area observed with ambient seismic noise. Geophys J Int 202, 920–932. https://doi.org/10.1093/gji/ggv151

Hillers, G., Campillo, M., Ma, K.-F., 2014. Seismic velocity variations at TCDP are controlled by MJO driven precipitation pattern and high fluid discharge properties. Earth and Planetary Science Letters 391, 121–127. https://doi.org/10.1016/j.epsl.2014.01.040

Hillers, G., Husen, S., Obermann, A., Planès, T., Larose, E., Campillo, M., 2015b. Noise-based monitoring and imaging of aseismic transient deformation induced by the 2006 Basel reservoir stimulation. GEOPHYSICS 80, KS51–KS68. https://doi.org/10.1190/geo2014-0455.1

Hillers, G., Retailleau, L., Campillo, M., Inbal, A., Ampuero, J.-P., Nishimura, T., 2015c. In situ observations of velocity changes in response to tidal deformation from analysis of the high-frequency ambient wavefield. Journal of Geophysical Research: Solid Earth 120, 210–225. https://doi.org/10.1002/2014JB011318

Hobiger, M., Wegler, U., Shiomi, K., Nakahara, H., 2016. Coseismic and post-seismic velocity changes detected by Passive Image Interferometry: comparison of one great and five strong earthquakes in Japan. Geophys J Int 205, 1053–1073. https://doi.org/10.1093/gji/ggw066

Hotovec‐Ellis, A.J., Gomberg, J., Vidale, J.E., Creager, K.C., 2014. A continuous record of intereruption velocity change at Mount St. Helens from coda wave interferometry. Journal of Geophysical Research: Solid Earth 119, 2199‐2214. https://doi.org/10.1002/2013JB010742

Huang, X., García, M.H., 1998. A Herschel–Bulkley model for mud flow down a slope. Journal of Fluid Mechanics 374, 305–333. https://doi.org/10.1017/S0022112098002845

Imposa, S., Grassi, S., Fazio, F., Rannisi, G., Cino, P., 2017. Geophysical surveys to study a landslide body (north-eastern Sicily). Nat Hazards 86, 327–343. https://doi.org/10.1007/s11069-016-2544-1

Intrieri, E., Carlà, T., Gigli, G., 2019. Forecasting the time of failure of landslides at slope-scale: A literature review. Earth-Science Reviews. https://doi.org/10.1016/j.earscirev.2019.03.019

Intrieri, E., Gigli, G., Mugnai, F., Fanti, R., Casagli, N., 2012. Design and implementation of a landslide early warning system. Engineering Geology 147–148, 124–136. https://doi.org/10.1016/j.enggeo.2012.07.017

Iverson, R.M., Reid, M.E., LaHusen, R.G., 1997. Debris-flow mobilization from landslides. Annual Review of Earth and Planetary Sciences 25, 85–138.

James, S.R., Knox, H.A., Abbott, R.E., Screaton, E.J., 2017. Improved moving window cross-spectral analysis for resolving large temporal seismic velocity changes in permafrost. Geophysical Research Letters 44, 4018–4026. https://doi.org/10.1002/2016GL072468

Jongmans, D., Bièvre, G., Schwartz, S., Renalier, F., Beaurez, N., 2009. Geophysical investigation of the large Avignonet landslide in glaciolacustrine clays in the Trièves area (French Alps). Engineering Geology 109, 45–56. https://doi.org/10.1016/j.enggeo.2008.10.005

Jongmans, D., Garambois, S., 2007. Geophysical investigation of landslides : a review. Bulletin de la Société Géologique de France 178, 101–112. https://doi.org/10.2113/gssgfbull.178.2.101

Joubert, A., Le Feuvre, M., Côte, P., 2018. Passive monitoring of a sea dike during a tidal cycle using sea waves as a seismic noise source. Geophys J Int 214, 1364–1378. https://doi.org/10.1093/gji/ggy180

Keefer, D.K., 1984. Landslides caused by earthquakes. Geological Society of America Bulletin 95, 406–421. https://doi.org/10.1130/0016-7606(1984)95<406:LCBE>2.0.CO;2

Kinar, N.J., Pomeroy, J.W., 2015. Measurement of the physical properties of the snowpack. Reviews of Geophysics 53, 481–544. https://doi.org/10.1002/2015RG000481

Kleinbrod, U., Burjánek, J., Fäh, D., 2019. Ambient vibration classification of unstable rock slopes: A systematic approach. Engineering Geology 249, 198–217. https://doi.org/10.1016/j.enggeo.2018.12.012

Konstantaki, L.A., Carpentier, S., Garofalo, F., Bergamo, P., Socco, L.V., 2013. Determining hydrological and soil mechanical parameters from multichannel surface‐wave analysis across the Alpine Fault at Inchbonnie, New Zealand. Near Surface Geophysics 11, 435–448. https://doi.org/10.3997/1873-0604.2013019

Lacroix, P., Grasso, J.-R., Roulle, J., Giraud, G., Goetz, D., Morin, S., Helmstetter, A., 2012. Monitoring of snow avalanches using a seismic array: Location, speed estimation, and relationships to meteorological variables. Journal of Geophysical Research: Earth Surface 117. https://doi.org/10.1029/2011JF002106

Lacroix, P., Helmstetter, A., 2011. Location of Seismic Signals Associated with Microearthquakes and Rockfalls on the Sechilienne Landslide, French Alps. Bulletin of the Seismological Society of America 101, 341–353. https://doi.org/10.1785/0120100110

Larose, E., 2004. Imaging from one-bit correlations of wideband diffuse wave fields. Journal of Applied Physics 95, 8393. https://doi.org/10.1063/1.1739529

Larose, E., Carrière, S., Voisin, C., Bottelin, P., Baillet, L., Guéguen, P., Walter, F., Jongmans, D., Guillier, B., Garambois, S., Gimbert, F., Massey, C., 2015. Environmental seismology: What can we learn on earth surface processes with ambient noise? Journal of Applied Geophysics 116, 62–74. https://doi.org/10.1016/j.jappgeo.2015.02.001

Larose, E., Derode, A., Clorennec, D., Margerin, L., Campillo, M., 2005. Passive retrieval of Rayleigh waves in disordered elastic media. Physical Review E 72. https://doi.org/10.1103/PhysRevE.72.046607

Larose, E., Hall, S., 2009. Monitoring stress related velocity variation in concrete with a 2×10−5 relative resolution using diffuse ultrasound. The Journal of the Acoustical Society of America 125, 1853–1856. https://doi.org/10.1121/1.3079771

Le Breton, M., 2019a. Suivi temporel d'un glissement de terrain à l'aide d'étiquettes RFID passives, couplé à l'observation de pluviométrie et de bruit sismique ambiant — chapter 8 — Impulse response from rainfall to displacement (PhD Thesis). Université Grenoble Alpes, ISTerre, Grenoble, France.

Le Breton, M., 2019b. Suivi temporel d'un glissement de terrain à l'aide d'étiquettes RFID passives, couplé à l'observation de pluviométrie et de bruit sismique ambiant. (Ph.D. Thesis). Grenoble Alpes, Grenoble.

Le Breton, M., Baillet, L., Larose, E., Rey, E., Benech, P., Jongmans, D., Guyoton, F., Jaboyedoff, M., 2019. Passive radio-frequency identification ranging, a dense and weather-robust technique for landslide displacement monitoring. Engineering Geology 250, 1–10. https://doi.org/10.1016/j.enggeo.2018.12.027

Lecocq, T., Hicks, S.P., Noten, K.V., Wijk, K. van, Koelemeijer, P., Plaen, R.S.M.D., Massin, F., Hillers, G., Anthony, R.E., Apoloner, M.-T., Arroyo-Solórzano, M., Assink, J.D., Büyükakpınar, P., Cannata, A., Cannavo, F., Carrasco, S., Caudron, C., Chaves, E.J., Cornwell, D.G., Craig, D., Ouden, O.F.C. den, Diaz, J., Donner, S., Evangelidis, C.P., Evers, L., Fauville, B., Fernandez, G.A., Giannopoulos, D., Gibbons, S.J., Girona, T., Grecu, B., Grunberg, M., Hetényi, G., Horleston, A., Inza, A., Irving, J.C.E., Jamalreyhani, M., Kafka, A., Koymans, M.R., Labedz, C.R., Larose, E., Lindsey, N.J., McKinnon, M., Megies, T., Miller, M.S., Minarik, W., Moresi, L., Márquez-Ramírez, V.H., Möllhoff, M., Nesbitt, I.M., Niyogi, S., Ojeda, J., Oth, A., Proud, S., Pulli, J., Retailleau, L., Rintamäki, A.E., Satriano, C., Savage, M.K., Shani-Kadmiel, S., Sleeman, R., Sokos, E., Stammler, K., Stott, A.E., Subedi, S., Sørensen, M.B., Taira, T., Tapia, M., Turhan, F., Pluijm, B. van der, Vanstone, M., Vergne, J., Vuorinen, T.A.T., Warren, T., Wassermann, J., Xiao, H., 2020. Global quieting of high-frequency seismic noise due to COVID-19 pandemic lockdown measures. Science. https://doi.org/10.1126/science.abd2438

Lecocq, T., Longuevergne, L., Pedersen, H.A., Brenguier, F., Stammler, K., 2017. Monitoring ground water storage at mesoscale using seismic noise: 30 years of continuous observation and thermo-elastic and hydrological modeling. Scientific Reports 7, 14241. https://doi.org/10.1038/s41598-017-14468-9

Lesage, P., Reyes‐Dávila, G., Arámbula‐Mendoza, R., 2014. Large tectonic earthquakes induce sharp temporary decreases in seismic velocity in Volcán de Colima, Mexico. Journal

of Geophysical Research: Solid Earth 119, 4360 - 4376. https://doi.org/10.1002/2013JB010884

Lévy, C., Baillet, L., Jongmans, D., Mourot, P., Hantz, D., 2010. Dynamic response of the Chamousset rock column (Western Alps, France). Journal of Geophysical Research 115. https://doi.org/10.1029/2009JF001606

Lobkis, O.I., Weaver, R.L., 2001. On the emergence of the Green's function in the correlations of a diffuse field. The Journal of the Acoustical Society of America 110, 3011–3017. https://doi.org/10.1121/1.1417528

Louie, J.N., 2001. Faster, Better: Shear-Wave Velocity to 100 Meters Depth from Refraction Microtremor Arrays. Bulletin of the Seismological Society of America 91, 347–364. https://doi.org/10.1785/0120000098

Machacca-Puma, R., Lesage, P., Larose, E., Lacroix, P., Anccasi-Figueroa, R.M., 2019a. Detection of pre-eruptive seismic velocity variations at an andesitic volcano using ambient noise correlation on 3-component stations: Ubinas volcano, Peru, 2014. Journal of Volcanology and Geothermal Research 381, 83–100. https://doi.org/10.1016/j.jvolgeores.2019.05.014

Machacca-Puma, R., Lesage, P., Larose, E., Lacroix, P., Anccasi-Figueroa, R.M., 2019b. Detection of pre-eruptive seismic velocity variations at an andesitic volcano using ambient noise correlation on 3-component stations: Ubinas volcano, Peru, 2014. Journal of Volcanology and Geothermal Research 381, 83–100. https://doi.org/10.1016/j.jvolgeores.2019.05.014

Mainsant, G., Chambon, G., Jongmans, D., Larose, E., Baillet, L., 2015. Shear-wave-velocity drop prior to clayey mass movement in laboratory flume experiments. Engineering Geology 192, 26–32. https://doi.org/10.1016/j.enggeo.2015.03.019

Mainsant, G., Jongmans, D., Chambon, G., Larose, E., Baillet, L., 2012a. Shear-wave velocity as an indicator for rheological changes in clay materials: Lessons from laboratory experiments. Geophys. Res. Lett. 39, L19301. https://doi.org/10.1029/2012GL053159

Mainsant, G., Larose, E., Brönnimann, C., Jongmans, D., Michoud, C., Jaboyedoff, M., 2012b. Ambient seismic noise monitoring of a clay landslide: Toward failure prediction. J. Geophys. Res. 117, F01030. https://doi.org/10.1029/2011JF002159

Mao, S., Campillo, M., Hilst, R.D. van der, Brenguier, F., Stehly, L., Hillers, G., 2019. High Temporal Resolution Monitoring of Small Variations in Crustal Strain by Dense Seismic Arrays. Geophysical Research Letters 46, 128–137. https://doi.org/10.1029/2018GL079944

Margerin, L., Campillo, M., Tiggelen, B.A.V., Hennino, R., 2009. Energy partition of seismic coda waves in layered media: theory and application to Pinyon Flats Observatory. Geophysical Journal International 177, 571–585. https://doi.org/10.1111/j.1365-246X.2008.04068.x

Massey, C.I., Petley, D.N., McSaveney, M.J., 2013. Patterns of movement in reactivated landslides. Engineering Geology 159, 1–19. https://doi.org/10.1016/j.enggeo.2013.03.011

McNamara, D.E., Boaz, R.I., 2019. Visualization of the Seismic Ambient Noise Spectrum, in: Seismic Ambient Noise. Cambridge University Press, Cambridge ; New York, NY.

McNamara, D.E., Buland, R.P., 2004. Ambient noise levels in the continental United States. Bulletin of the seismological society of America 94, 1517–1527.

Mehta, K., Snieder, R., Graizer, V., 2007. Downhole Receiver Function: a Case Study. Bulletin of the Seismological Society of America 97, 1396–1403. https://doi.org/10.1785/0120060256

Meier, U., Shapiro, N.M., Brenguier, F., 2010. Detecting seasonal variations in seismic velocities within Los Angeles basin from correlations of ambient seismic noise. Geophysical Journal International 181, 985–996. https://doi.org/10.1111/j.1365-246X.2010.04550.x

Méric, O., Garambois, S., Malet, J.-P., Cadet, H., Guéguen, P., Jongmans, D., 2007. Seismic noise-based methods for soft-rock landslide characterization. Bulletin de la Société Géologique de France 178, 137–148. https://doi.org/10.2113/gssgfbull.178.2.137

Miao, Y., Shi, Y., Wang, S.-Y., 2018. Temporal change of near-surface shear wave velocity associated with rainfall in Northeast Honshu, Japan. Earth Planets Space 70, 204. https://doi.org/10.1186/s40623-018-0969-3

Miao, Y., Shi, Y., Zhuang, H.Y., Wang, S.Y., Liu, H.B., Yu, X.B., 2019. Influence of Seasonal Frozen Soil on Near-Surface Shear Wave Velocity in Eastern Hokkaido, Japan. Geophysical Research Letters 46, 9497–9508. https://doi.org/10.1029/2019GL082282

Mikesell, T.D., Malcolm, A.E., Yang, D., Haney, M.M., 2015. A comparison of methods to estimate seismic phase delays: numerical examples for coda wave interferometry. Geophys J Int 202, 347–360. https://doi.org/10.1093/gji/ggv138

Mordret, A., Mikesell, T.D., Harig, C., Lipovsky, B.P., Prieto, G.A., 2016. Monitoring southwest Greenland's ice sheet melt with ambient seismic noise. Science Advances 2, e1501538. https://doi.org/10.1126/sciadv.1501538

Moreau, L., Stehly, L., Boué, P., Lu, Y., Larose, E., Campillo, M., 2017. Improving ambient noise correlation functions with an SVD-based Wiener filter. Geophys J Int 211, 418–426. https://doi.org/10.1093/gji/ggx306

Nakahara, H., 2015. Auto Correlation Analysis of Coda Waves from Local Earthquakes for Detecting Temporal Changes in Shallow Subsurface Structures: the 2011 Tohoku-Oki, Japan Earthquake. Pure Appl. Geophys. 172, 213–224. https://doi.org/10.1007/s00024-014-0849-0

Nakamura, Y., 1989. A METHOD FOR DYNAMIC CHARACTERISTICS ESTIMATION OF SUBSURFACE USING MICROTREMOR ON THE GROUND SURFACE. Railway Technical Research Institute, Quarterly Reports 30.

Nakata, N., Boué, P., Brenguier, F., Roux, P., Ferrazzini, V., Campillo, M., 2016. Body and surface wave reconstruction from seismic noise correlations between arrays at Piton de la Fournaise volcano. Geophysical Research Letters 43, 1047–1054. https://doi.org/10.1002/2015GL066997

Nakata, N., Snieder, R., 2012. Estimating near-surface shear wave velocities in Japan by applying seismic interferometry to KiK-net data. Journal of Geophysical Research: Solid Earth 117. https://doi.org/10.1029/2011JB008595

Nakata, N., Snieder, R., 2011. Near-surface weakening in Japan after the 2011 Tohoku-Oki earthquake. Geophysical Research Letters 38. https://doi.org/10.1029/2011GL048800

Obermann, A., Froment, B., Campillo, M., Larose, E., Planès, T., Valette, B., Chen, J.H., Liu, Q.Y., 2014. Seismic noise correlations to image structural and mechanical changes associated with the Mw 7.9 2008 Wenchuan earthquake. Journal of Geophysical Research: Solid Earth 119, 3155–3168. https://doi.org/10.1002/2013JB010932

Obermann, A., Planès, T., Hadziioannou, C., Campillo, M., 2016. Lapse-time-dependent coda-wave depth sensitivity to local velocity perturbations in 3-D heterogeneous elastic media. Geophys J Int 207, 59–66. https://doi.org/10.1093/gji/ggw264

Obermann, A., Planès, T., Larose, E., Campillo, M., 2019. 4-D Imaging of Subsurface Changes with Coda Waves: Numerical Studies of 3-D Combined Sensitivity Kernels and Applications to the $$M_{\mathrm{w}}$$Mw7.9, 2008 Wenchuan Earthquake. Pure Appl. Geophys. 176, 1243–1254. https://doi.org/10.1007/s00024-018-2014-7

Obermann, A., Planès, T., Larose, E., Campillo, M., 2013a. Imaging preeruptive and coeruptive structural and mechanical changes of a volcano with ambient seismic noise. Journal of Geophysical Research: Solid Earth 118, 6285–6294. https://doi.org/10.1002/2013JB010399

Obermann, A., Planès, T., Larose, E., Sens-Schönfelder, C., Campillo, M., 2013b. Depth sensitivity of seismic coda waves to velocity perturbations in an elastic heterogeneous medium. Geophys J Int 194, 372–382. https://doi.org/10.1093/gji/ggt043

Olivier, G., Brenguier, F., de Wit, T., Lynch, R., 2017. Monitoring the stability of tailings dam walls with ambient seismic noise. The Leading Edge 36, 350a1-350a6. https://doi.org/10.1190/tle36040350a1.1

Ostrovsky, L.A., Johnson, P.A., 2001. Dynamic nonlinear elasticity in geo materials. Rivista del Nuovo Cimento della Societa Italiana di Fisica 24, 1–46.

Paasschens, J.C.J., 1997. Solution of the time-dependent Boltzmann equation. Phys. Rev. E 56, 1135–1141. https://doi.org/10.1103/PhysRevE.56.1135

Park, C.B., Miller, R.D., Xia, J., 1999. Multichannel analysis of surface waves. GEOPHYSICS 64, 800–808. https://doi.org/10.1190/1.1444590

Pazzi, V., Tanteri, L., Bicocchi, G., D'Ambrosio, M., Caselli, A., Fanti, R., 2017. H/V measurements as an effective tool for the reliable detection of landslide slip surfaces: Case studies of Castagnola (La Spezia, Italy) and Roccalbegna (Grosseto, Italy). Physics and Chemistry of the Earth, Parts A/B/C, Advance in seismic site response: usual practices and innovative methods 98, 136–153. https://doi.org/10.1016/j.pce.2016.10.014

Peterson, J.R., 1993. Observations and modeling of seismic background noise (USGS Numbered Series No. 93–322), Open-File Report. U.S. Geological Survey.

Pilz, M., Parolai, S., Bindi, D., Saponaro, A., Abdybachaev, U., 2014. Combining Seismic Noise Techniques for Landslide Characterization. Pure Appl. Geophys. 171, 1729–1745. https://doi.org/10.1007/s00024-013-0733-3

Pirazzini, R., Leppänen, L., Picard, G., Lopez-Moreno, J.I., Marty, C., Macelloni, G., Kontu, A., von Lerber, A., Tanis, C.M., Schneebeli, M., de Rosnay, P., Arslan, A.N., 2018. European In-Situ Snow Measurements: Practices and Purposes. Sensors (Basel) 18. https://doi.org/10.3390/s18072016

Planès, T., Larose, E., Rossetto, V., Margerin, L., 2015. Imaging multiple local changes in heterogeneous media with diffuse waves. The Journal of the Acoustical Society of America 137, 660–667. https://doi.org/10.1121/1.4906824

Planès, T., Mooney, M.A., Rittgers, J.B.R., Parekh, M.L., Behm, M., Snieder, R., 2016. Time-lapse monitoring of internal erosion in earthen dams and levees using ambient seismic noise. Géotechnique 66, 301–312. https://doi.org/10.1680/jgeot.14.P.268

Planès, T., Rittgers, J.B., Mooney, M.A., Kanning, W., Draganov, D., 2017. Monitoring the tidal response of a sea levee with ambient seismic noise. Journal of Applied Geophysics 138, 255–263. https://doi.org/10.1016/j.jappgeo.2017.01.025

Poli, P., 2017. Creep and slip: Seismic precursors to the Nuugaatsiaq landslide (Greenland). Geophysical Research Letters 44, 8832–8836. https://doi.org/10.1002/2017GL075039

Preiswerk, L.E., Walter, F., 2018. High-Frequency (>2 Hz) Ambient Seismic Noise on High-Melt Glaciers: Green's Function Estimation and Source Characterization. Journal of Geophysical Research: Earth Surface 123, 1667–1681. https://doi.org/10.1029/2017JF004498

Provost, F., Hibert, C., Malet, J.-P., 2017. Automatic classification of endogenous landslide seismicity using the Random Forest supervised classifier: SEISMIC SOURCES AUTOMATIC CLASSIFICATION. Geophys. Res. Lett. 44, 113–120. https://doi.org/10.1002/2016GL070709

Provost, F., Malet, J.-P., Gance, J., Helmstetter, A., Doubre, C., 2018a. Automatic approach for increasing the location accuracy of slow-moving landslide endogenous seismicity: the APOLoc method. Geophys J Int 215, 1455–1473. https://doi.org/10.1093/gji/ggy330

Provost, F., Malet, J.P., Hibert, C., Helmstetter, A., Radiguet, M., Amitrano, D., Langet, N., Larose, E., Abancó, C., Hürlimann, M., Lebourg, T., Levy, C., Le Roy, G., Ulrich, P., Vidal, M., Vial, B., 2018b. Towards a standard typology of endogenous landslide seismic sources. Earth Surface Dynamics 6, 1059–1088. https://doi.org/10.5194/esurf-6-1059-2018

Rankinen, K., Karvonen, T., Butterfield, D., 2004. A simple model for predicting soil temperature in snow-covered and seasonally frozen soil: model description and testing. Hydrology and Earth System Sciences 8, 706–716. https://doi.org/10.5194/hess-8-706-2004

Ratdomopurbo, A., Poupinet, G., 1995. Monitoring a temporal change of seismic velocity in a volcano: Application to the 1992 eruption of Mt. Merapi (Indonesia). Geophysical Research Letters 22, 775–778. https://doi.org/10.1029/95GL00302

Renalier, F., Bièvre, G., Jongmans, D., Campillo, M., Bard, P.-Y., 2010a. Clayey Landslide Investigations Using Active and Passive VS Measurements, in: Advances in Near-Surface Seismology and Ground-Penetrating Radar. Society of Exploration Geophysicists, American Geophysical Union, Environmental and Engineering Geophysical Society, pp. 397–413. https://doi.org/10.1190/1.9781560802259.ch24

Renalier, F., Jongmans, D., Campillo, M., Bard, P.-Y., 2010b. Shear wave velocity imaging of the Avignonet landslide (France) using ambient noise cross correlation. Journal of Geophysical Research: Earth Surface 115. https://doi.org/10.1029/2009JF001538

Revil, A., Soueid Ahmed, A., Coperey, A., Ravanel, L., Sharma, R., Panwar, N., 2020. Induced polarization as a tool to characterize shallow landslides. Journal of Hydrology 589, 125369. https://doi.org/10.1016/j.jhydrol.2020.125369

Richter, T., Sens‐Schönfelder, C., Kind, R., Asch, G., 2014. Comprehensive observation and modeling of earthquake and temperature-related seismic velocity changes in northern Chile with passive image interferometry. Journal of Geophysical Research: Solid Earth 119, 4747–4765. https://doi.org/10.1002/2013JB010695

Ritzwoller, M.H., Feng, L., 2019. Overview of Pre- and Post-Processing of Ambient-Noise Correlations., in: Nakata, N., Gualtieri, L., Fichtner, A. (Eds.), Seismic Ambient Noise. Cambridge University Press., Cambridge, pp. 144–187.

Rivet, D., Brenguier, F., Cappa, F., 2015. Improved detection of preeruptive seismic velocity drops at the Piton de La Fournaise volcano. Geophysical Research Letters 42, 6332–6339. https://doi.org/10.1002/2015GL064835

Rivet, D., Brenguier, F., Clarke, D., Shapiro, N.M., Peltier, A., 2014. Long-term dynamics of Piton de la Fournaise volcano from 13 years of seismic velocity change measurements and GPS observations. Journal of Geophysical Research: Solid Earth 119, 7654–7666. https://doi.org/10.1002/2014JB011307

Rivet, D., Campillo, M., Shapiro, N.M., Cruz‐Atienza, V., Radiguet, M., Cotte, N., Kostoglodov, V., 2011. Seismic evidence of nonlinear crustal deformation during a large slow slip event in Mexico. Geophysical Research Letters 38. https://doi.org/10.1029/2011GL047151

Rojstaczer, S., Wolf, S., 1992. Permeability changes associated with large earthquakes: An example from Loma Prieta, California. Geology 20, 211–214. https://doi.org/10.1130/0091-7613(1992)020<0211:PCAWLE>2.3.CO;2

Sabra, K.G., Roux, P., Thode, A.M., D'Spain, G.L., Hodgkiss, W.S., Kuperman, W.A., 2005. Using ocean ambient noise for array self-localization and self-synchronization. IEEE Journal of Oceanic Engineering 30, 338–347. https://doi.org/10.1109/JOE.2005.850908

Schöpa, A., Chao, W.-A., Lipovsky, B.P., Hovius, N., White, R.S., Green, R.G., Turowski, J.M., 2018. Dynamics of the Askja caldera July 2014 landslide, Iceland, from seismic signal analysis: precursor, motion and aftermath. Earth Surface Dynamics 6, 467–485. https://doi.org/10.5194/esurf-6-467-2018

Schulz, W.H., Kean, J.W., Wang, G., 2009. Landslide movement in southwest Colorado triggered by atmospheric tides. Nature Geoscience 2, 863–866. https://doi.org/10.1038/ngeo659

Seiler, K.-P., Gat, J.R., 2007. Groundwater Recharge from Run-Off, Infiltration and Percolation, Water Science and Technology Library. Springer Netherlands, Dordrecht. https://doi.org/10.1007/978-1-4020-5306-1

Senfaute, G., Duperret, A., Lawrence, J.A., 2009. Micro-seismic precursory cracks prior to rock-fall on coastal chalk cliffs: a case study at Mesnil-Val, Normandie, NW France. Natural Hazards and Earth System Science 9, 1625–1641. https://doi.org/10.5194/nhess-9-1625-2009

Sens-Schönfelder, C., 2008. Synchronizing seismic networks with ambient noise. Geophys J Int 174, 966–970. https://doi.org/10.1111/j.1365-246X.2008.03842.x

Sens-Schönfelder, C., Brenguier, F., 2019. Noise-Based Monitoring, in: Seismic Ambient Noise. Cambridge University Press.

Sens-Schönfelder, C., Larose, E., 2008. Temporal changes in the lunar soil from correlation of diffuse vibrations. Phys. Rev. E 78, 045601. https://doi.org/10.1103/PhysRevE.78.045601

Sens-Schönfelder, C., Wegler, U., 2006. Passive image interferometry and seasonal variations of seismic velocities at Merapi Volcano, Indonesia. Geophys. Res. Lett. 33, L21302. https://doi.org/10.1029/2006GL027797

Shapiro, N.M., Campillo, M., 2004. Emergence of broadband Rayleigh waves from correlations of the ambient seismic noise. Geophysical Research Letters 31. https://doi.org/10.1029/2004GL019491

Shapiro, N.M., Campillo, M., Margerin, L., Singh, S.K., Kostoglodov, V., Pacheco, J., 2000. The Energy Partitioning and the Diffusive Character of the Seismic Coda. Bulletin of the Seismological Society of America 90, 655–665. https://doi.org/10.1785/0119990021

Snieder, R., Larose, E., 2013. Extracting Earth's Elastic Wave Response from Noise Measurements. Annual Review of Earth and Planetary Sciences 41, 183–206. https://doi.org/10.1146/annurev-earth-050212-123936

Snieder, R., Safak, E., 2006. Extracting the building response using seismic interferometry: Theory and application to the Millikan Library in Pasadena, California. Bulletin of the Seismological Society of America 96, 13. https://doi.org/10.1785/0120050109

Snieder, R., Sens-Schönfelder, C., Wu, R., 2017. The time dependence of rock healing as a universal relaxation process, a tutorial. Geophys. J. Int. 208, 1–9. https://doi.org/10.1093/gji/ggw377

Spillmann, T., Maurer, H., Green, A.G., Heincke, B., Willenberg, H., Husen, S., 2007a. Microseismic investigation of an unstable mountain slope in the Swiss Alps. Journal of Geophysical Research: Solid Earth 112. https://doi.org/10.1029/2006JB004723

Spillmann, T., Maurer, H., Green, A.G., Heincke, B., Willenberg, H., Husen, S., 2007b. Microseismic investigation of an unstable mountain slope in the Swiss Alps. Journal of Geophysical Research: Solid Earth 112. https://doi.org/10.1029/2006JB004723

Staub, B., Delaloye, R., 2017. Using Near-Surface Ground Temperature Data to Derive Snow Insulation and Melt Indices for Mountain Permafrost Applications. Permafrost and Periglacial Processes 28, 237–248. https://doi.org/10.1002/ppp.1890

Stehly, L., Campillo, M., Froment, B., Weaver, R.L., 2008. Reconstructing Green's function by correlation of the coda of the correlation (C3) of ambient seismic noise. Journal of Geophysical Research: Solid Earth 113. https://doi.org/10.1029/2008JB005693

Stehly, L., Campillo, M., Shapiro, N.M., 2007. Traveltime measurements from noise correlation: stability and detection of instrumental time-shifts. Geophys J Int 171, 223–230. https://doi.org/10.1111/j.1365-246X.2007.03492.x

Stehly, L., Campillo, M., Shapiro, N.M., 2006. A study of the seismic noise from its long-range correlation properties. Journal of Geophysical Research: Solid Earth 111. https://doi.org/10.1029/2005JB004237

Suriñach, E., Vilajosana, I., Khazaradze, G., Biescas, B., Furdada, G., Vilaplana, J.M., 2005. Seismic detection and characterization of landslides and other mass movements. Natural Hazards and Earth System Science 5, 791–798.

Taira, T., Brenguier, F., 2016. Response of hydrothermal system to stress transients at Lassen Volcanic Center, California, inferred from seismic interferometry with ambient noise. Earth, Planets and Space 68, 162. https://doi.org/10.1186/s40623-016-0538-6

Takano, T., Nishimura, T., Nakahara, H., Ohta, Y., Tanaka, S., 2014. Seismic velocity changes caused by the Earth tide: Ambient noise correlation analyses of small-array data. Geophysical Research Letters 41, 6131–6136. https://doi.org/10.1002/2014GL060690

Takano, T., Nishimura, T., Nakahara, H., Ueda, H., Fujita, E., 2019. Sensitivity of Seismic Velocity Changes to the Tidal Strain at Different Lapse Times: Data Analyses of a Small Seismic Array at Izu‐Oshima Volcano. J. Geophys. Res. Solid Earth 124, 3011‐3023. https://doi.org/10.1029/2018JB016235

Tedesco, M., 2015. Remote Sensing of the Cryosphere, 1st ed, The Cryosphere Science Series. Wiley.

TenCate, J.A., 2011. Slow Dynamics of Earth Materials: An Experimental Overview. Pure Appl. Geophys. 168, 2211–2219. https://doi.org/10.1007/s00024-011-0268-4

Thery, R., Guillemot, A., Abraham, O., Larose, E., 2019. Tracking fluids in multiple scattering and highly porous materials: toward applications in non-destructive testing and seismic monitoring. Ultrasonics 106019. https://doi.org/10.1016/j.ultras.2019.106019

Tonnellier, A., Helmstetter, A., Malet, J.-P., Schmittbuhl, J., Corsini, A., Joswig, M., 2013. Seismic monitoring of soft-rock landslides: the Super-Sauze and Valoria case studies. Geophys. J. Int. 193, 1515–1536. https://doi.org/10.1093/gji/ggt039

Tournat, V., Zaitsev, V., Gusev, V., Nazarov, V., Béquin, P., Castagnède, B., 2004. Probing weak forces in granular media through nonlinear dynamic dilatancy: clapping contacts and polarization anisotropy. Physical review letters 92, 085502.

Tsai, V.C., 2011. A model for seasonal changes in GPS positions and seismic wave speeds due to thermoelastic and hydrologic variations. Journal of Geophysical Research: Solid Earth 116. https://doi.org/10.1029/2010JB008156

Valentin, J., 2018. Suivi de glissements rocheux et de coulées dans les roches argileuses à partir de méthodes sismiques et photogrammétriques (thesis). Grenoble Alpes.

Valentin, J., Capron, A., Jongmans, D., Baillet, L., Bottelin, P., Donze, F., Larose, E., Mangeney, A., 2017. The dynamic response of prone-to-fall columns to ambient vibrations: comparison between measurements and numerical modelling. Geophys J Int 208, 1058–1076. https://doi.org/10.1093/gji/ggw440

Van Asch, T.W.J., Malet, J.-P., 2009. Flow-type failures in fine-grained soils: an important aspect in landslide hazard analysis. Natural Hazards and Earth System Sciences 9, 1703–1711. https://doi.org/10.5194/nhess-9-1703-2009

van Herwijnen, A., Schweizer, J., 2011. Monitoring avalanche activity using a seismic sensor. Cold Regions Science and Technology, International Snow Science Workshop 2010 Lake Tahoe 69, 165–176. https://doi.org/10.1016/j.coldregions.2011.06.008

Viens, L., Denolle, M.A., Hirata, N., Nakagawa, S., 2018. Complex Near-Surface Rheology Inferred From the Response of Greater Tokyo to Strong Ground Motions. Journal of Geophysical Research: Solid Earth 123, 5710–5729. https://doi.org/10.1029/2018JB015697

Voisin, C., Garambois, S., Massey, C., Brossier, R., 2016. Seismic noise monitoring of the water table in a deep-seated, slow-moving landslide. Interpretation 4, SJ67–SJ76. https://doi.org/10.1190/INT-2016-0010.1

Voisin, C., Guzmán, M.A.R., Réfloch, A., Taruselli, M., Garambois, S., 2017. Groundwater Monitoring with Passive Seismic Interferometry. Journal of Water Resource and Protection 09, 1414. https://doi.org/10.4236/jwarp.2017.912091

Vouillamoz, N., Rothmund, S., Joswig, M., 2018. Characterizing the complexity of microseismic signals at slow-moving clay-rich debris slides: the Super-Sauze (southeastern France) and Pechgraben (Upper Austria) case studies. Earth Surface Dynamics 6, 525–550. https://doi.org/10.5194/esurf-6-525-2018

Walter, F., Roux, P., Roeoesli, C., Lecointre, A., Kilb, D., Roux, P.-F., 2015. Using glacier seismicity for phase velocity measurements and Green's function retrieval. Geophys J Int 201, 1722–1737. https://doi.org/10.1093/gji/ggv069

Walter, M., Arnhardt, C., Joswig, M., 2011. Seismic monitoring of rockfalls, slide quakes, and fissure development at the Super-Sauze mudslide, French Alps. Engineering Geology 128, 12–22. https://doi.org/10.1016/j.enggeo.2011.11.002

Walter, M., Gomberg, J., Schulz, W., Bodin, P., Joswig, M., 2013. Slidequake Generation versus Viscous Creep at Softrock-landslides: Synopsis of Three Different Scenarios at Slumgullion Landslide, Heumoes Slope, and Super-Sauze Mudslide. Journal of Environmental & Engineering Geophysics 18, 269–280. https://doi.org/10.2113/JEEG18.4.269

Walter, M., Joswig, M., 2008. Seismic monitoring of fracture processes generated by a creeping landslide in the Vorarlberg Alps. First Break 26. https://doi.org/EAGE-EXPORT-FAKE-DOI

Wang, Baoshan, Zhu, P., Chen, Y., Niu, F., Wang, Bin, 2008. Continuous subsurface velocity measurement with coda wave interferometry. Journal of Geophysical Research: Solid Earth 113. https://doi.org/10.1029/2007JB005023

Wang, G., Sassa, K., 2003. Pore-pressure generation and movement of rainfall-induced landslides: effects of grain size and fine-particle content. Engineering Geology 69, 109–125. https://doi.org/10.1016/S0013-7952(02)00268-5

Wang, Q.-Y., Brenguier, F., Campillo, M., Lecointre, A., Takeda, T., Aoki, Y., 2017. Seasonal Crustal Seismic Velocity Changes Throughout Japan. Journal of Geophysical Research: Solid Earth 122, 7987–8002. https://doi.org/10.1002/2017JB014307

Wapenaar, K., Draganov, D., Snieder, R., Campman, X., Verdel, A., 2010. Tutorial on seismic interferometry: Part 1 — Basic principles and applications. GEOPHYSICS 75, 75A195-75A209. https://doi.org/10.1190/1.3457445

Wathelet, M., Jongmans, D., Ohrnberger, M., Bonnefoy-Claudet, S., 2008. Array performances for ambient vibrations on a shallow structure and consequences over V s inversion. J Seismol 12, 1–19. https://doi.org/10.1007/s10950-007-9067-x

Weaver, R.L., Hadziioannou, C., Larose, E., Campillo, M., 2011a. On the precision of noise correlation interferometry. Geophys J Int 185, 1384–1392. https://doi.org/10.1111/j.1365-246X.2011.05015.x

Weaver, R.L., Hadziioannou, C., Larose, E., Campillo, M., 2011b. On the precision of noise correlation interferometry. Geophys J Int 185, 1384–1392. https://doi.org/10.1111/j.1365-246X.2011.05015.x

Wegler, U., Lühr, B.G., 2001. Scattering behaviour at Merapi volcano (Java) revealed from an active seismic experiment. Geophys J Int 145, 579–592. https://doi.org/10.1046/j.1365-246x.2001.01390.x

Wegler, U., Sens‐Schönfelder, C., 2007. Fault zone monitoring with passive image interferometry. Geophys J Int 168, 1029‐1033. https://doi.org/10.1111/j.1365-246X.2006.03284.x

Whiteley, J.S., Chambers, J.E., Uhlemann, S., Wilkinson, P.B., Kendall, J.M., 2019. Geophysical Monitoring of Moisture-Induced Landslides: A Review. Reviews of Geophysics 57, 106–145. https://doi.org/10.1029/2018RG000603

Winkler, K., Nur, A., 1979. Pore fluids and seismic attenuation in rocks. Geophysical Research Letters 6, 1–4. https://doi.org/10.1029/GL006i001p00001

Withers, M.M., Aster, R.C., Young, C.J., Chael, E.P., 1996. High-frequency analysis of seismic background noise as a function of wind speed and shallow depth. Bulletin of the Seismological Society of America 86, 1507–1515.

Yamada, M., Mori, J., Matsushi, Y., 2016. Possible stick-slip behavior before the Rausu landslide inferred from repeating seismic events. Geophysical Research Letters 43, 9038–9044. https://doi.org/10.1002/2016GL069288

Yamamura, K., Sano, O., Utada, H., Takei, Y., Nakao, S., Fukao, Y., 2003. Long-term observation of in situ seismic velocity and attenuation. Journal of Geophysical Research: Solid Earth 108. https://doi.org/10.1029/2002JB002005

Young, C.J., Chael, E.P., Withers, M.M., Aster, R.C., n.d. A Comparison of the High-Frequency (> 1 Hz) Surface and Subsurface Noise Environment at Three Sites in the United States 13.

Zerathe, S., Lacroix, P., Jongmans, D., Marino, J., Taipe, E., Wathelet, M., Pari, W., Smoll, L.F., Norabuena, E., Guillier, B., Tatard, L., 2016. Morphology, structure and kinematics of a

rainfall controlled slow-moving Andean landslide, Peru. Earth Surface Processes and Landforms 41, 1477–1493. https://doi.org/10.1002/esp.3913

Zhan, Z., Tsai, V.C., Clayton, R.W., 2013. Spurious velocity changes caused by temporal variations in ambient noise frequency content. Geophys J Int 194, 1574–1581. https://doi.org/10.1093/gji/ggt170